

Evaluation of the Impacts of Rain Gauge Density and Distribution on Gauge-Satellite Merged Precipitation Estimates

Yuanyuan Chen, Jingfeng Huang[✉], Xiaodong Song[✉], Huayang Wen, and Haiyu Song

Abstract—The capacity of combined gauge-satellite precipitation estimates largely depends on the characteristics of the input data such as the number, location and reliability of rain gauges, and satellite-derived precipitation quality. The objective of this study is to examine the influence of rain gauge network configuration including density and spatial distribution on the performance of the gauge-satellite merging estimation at monthly and ten-day temporal scales. Dense rain gauge observations and satellite-derived precipitation data (i.e., TMPA 3B42 Version 7 and Version 06 IMERG Final Run) in two provinces of China are used. A two-stage downscaling-integration approach is applied in the gauge-satellite precipitation estimation. Various scenarios of rain gauge density and combination are designed and their corresponding merged precipitation estimates are evaluated using statistical indices. The merged results using the TMPA and IMERG precipitation product, respectively, are compared. The results show that: 1) the influence of rain gauge network configuration on the gauge-satellite merged precipitation estimates gradually decreases with the increase in rain gauge density, and the gauge-satellite merged precipitation estimates are more sensitive to the rain gauge network density in wet season and ten-day temporal scale than in dry season and monthly scale, respectively and 2) the merged precipitation estimation using the IMERG precipitation data generally outperforms the estimation using TMPA precipitation data in the low gauge

density scenarios, and the gap decreases with the increase in the rain gauge network density. In the areas with sparse rain gauges, improving the quality of satellite precipitation data would significantly improve the performance of the gauge-satellite merging estimation.

Index Terms—Downscaling-integration, gauge-satellite merged precipitation estimates, precipitation, rain gauge density, rain gauge spatial distribution.

I. INTRODUCTION

PRECIPITATION is a key element in the global water cycle. Acquiring accurate precipitation data sets with high spatiotemporal resolutions is crucial for water management, hydrological modeling, and predictions and is still a challenging task [1]. Conventional *in-situ* measurements from rain gauges could provide accurate precipitation information at rain gauge locations but lack spatial representation due to large spatial heterogeneity and relatively sparse distribution particularly in mountainous areas [2]. The satellite-derived precipitation products, for example, GPCP, PERSIANN, TMPA, and GSMaP, are attractive alternatives to detect spatial patterns of precipitation and have been widely applied in various applications [3]–[8]. However, the satellite-derived precipitation products usually contain large random and systematic errors affected by factors such as retrieval algorithms and topographic features [9]–[13]. Therefore, effectively combining multi-source precipitation data and developing high-quality, high-resolution precipitation products are necessary for hydrometeorological services and scientific research.

Since 1990s, great efforts have been made to integrate multisource precipitation data, and a series of global precipitation products have been developed. For example, the Global Precipitation Climatology Project (GPCP) and the Climate Precipitation Center (CPC) provide global precipitation analyses combining multiple satellite-based data with rain gauge analyses, including numerical model outputs [4], [13]–[15]. The widely used TMPA 3B43 product (Version 7) over 50°S–50°N has also been adjusted by monthly rain-gauge analysis of the Global Precipitation Climatology Centre (GPCC) [5]. These merged analyses have been widely used in meteorological monitoring, climate change analysis, and hydrological studies [16]–[19]. However, the improvements of the performance of these products are limited by restricted accessibility to rain gauge data [20], [21]. Although higher

Manuscript received August 14, 2020; revised October 8, 2020; accepted October 29, 2020. Date of publication November 24, 2020; date of current version December 2, 2021. This work was supported in part by the National Natural Science Foundation of China under Grant 41901363 and Grant 62073284, in part by the Erasmus + Programme of the European Union under Grant 598838-EPP-1-2018-EL-EPPKA2-CBHE-JP, in part by the Special Fund for Industrial and Scientific Research in the Public Interest (Meteorology) under Grant GYHY201406028, in part by the National Key Research and Development Program of China under Grant 2017YFD0300402-3, in part by the Department of Water Resources of Zhejiang Province through the Science and Technology Projects in 2018 under Grant RC1810, and in part by the Zhejiang Provincial Natural Science Foundation of China under Grant LY19F030008. (Corresponding author: Jingfeng Huang.)

Yuanyuan Chen is with the College of Environment, Zhejiang University of Technology, Hangzhou 310014, China, and also with the School of Information Management of Artificial Intelligence, Zhejiang University of Finance and Economics, Hangzhou 310018, China (e-mail: yyc@zufe.edu.cn).

Jingfeng Huang is with the Institute of Applied Remote Sensing and Information Technology, Zhejiang University, Hangzhou 310058, China (e-mail: hjf@zju.edu.cn).

Xiaodong Song is with the College of Geomatics and Municipal Engineering, Zhejiang University of Water Resources and Electric Power, Hangzhou 310018, China (e-mail: songxd@zjweu.edu.cn).

Huayang Wen is with Anhui Meteorological Information Centre, Hefei 230031, China (e-mail: wenhy12@163.com).

Haiyu Song is with the School of Information Management of Artificial Intelligence, Zhejiang University of Finance and Economics, Hangzhou 310018, China (e-mail: hysong@zufe.edu.cn).

Digital Object Identifier 10.1109/TGRS.2020.3037099

resolution products such as GSDMap-MVK, CMORPH Blended, and IMERG Final Run have been developed, the spatial resolution of these merged analyses still cannot meet the needs of hydrological and meteorological applications at local or regional scales [22], [23].

Over the past decades, numerous merging schemes, for example, objective analysis [24], [25], optimal interpolation techniques [26], [27], conditional merging [28], double kernel smoothing [29], inverse-root-mean-square-error weighting approach [30], geographical analysis [31]–[35], Bayesian merging and Kalman filtering [36]–[39], and multiscale analysis [40], [41], have been developed to merge multisource precipitation data. Among them, geographical-based merging schemes are one of the mainstream methods of merging multisource precipitation data because of their unique advantages in spatial statistical analysis and estimation and in spatial uncertainty estimation. Though combining satellite-derived precipitation with rain gauge observations can effectively improve the accuracy of precipitation estimates, there still exist obvious uncertainties rooted in merging algorithms themselves, input sources, the scale mismatch of different supports, and the spatial and temporal variability of precipitation [23], [29], [31], [42]. Verdin *et al.* [31], [37] pointed out that the Gaussian assumption of the Bayesian kriging approach could generate negative precipitation estimates in very dry areas and would be invalid at fine temporal scales, and the local polynomial scheme was much more sensitive to extrapolation and edge effects than the kriging model. Li and Shao [29] observed that directly merging rain gauge observations and coarse resolution satellite data could produce significant boundary biases in higher resolutions. The results of our previous work showed that the gauge-satellite merged precipitation estimates could be improved by downscaling the coarse resolution TMPA precipitation data to fine spatial resolution, and the accuracy significantly and positively correlated with the accuracy of satellite-derived precipitation while it negatively correlated with the spatial heterogeneity of precipitation [23].

The rain gauge observations are important input sources both in gauge-based precipitation estimates and gauge-satellite/radar precipitation merging estimates. The network density and spatial distribution of rain gauges have great influences on the precipitation estimation [43], [44]. Many studies have analyzed the effects of the rain gauge networks on the gauge-based areal precipitation estimates and lumped hydrological simulations [48]–[52]. Stihlreiter *et al.* [45] evaluated the performances of the total annual precipitation estimations and the runoff simulations of the HSAMI hydrological model with sparse and dense gauge networks, respectively. They observed that the total annual precipitation estimates and the runoff simulations could be improved with a denser gauge network. Xu *et al.* [46] found that the errors of the gauge-based areal rainfall and simulated runoff increased as the rain gauge number decreased. Lopez *et al.* [47] showed that the performance of the gauge-based precipitation estimation improved as the number of rain gauges increased and gradually leveled off. Recently, a few studies have quantitatively evaluated the influence of the rain gauge network density on

precipitation estimates by merging multiplatform information. For example, Berndt *et al.* [44] found that kriging with external drift had similar performance with the conditional merging in low rain-gauge density scenarios. Baik *et al.* [32] applied three different merging schemes to improve the gauge-satellite merged precipitation estimation at five rain gauge densities and various accumulation times. They showed that the accuracy of the merged results increased with the increase in the accumulation time and network density, and a similar work could be found by Park *et al.* [42]. In these studies, few rain gauge network density scenarios were designed, and the analyses of the influence of rain gauge location on the precipitation estimation are deficient. To better understand the influence of the spatial configuration of rain gauge on the gauge-satellite merged precipitation estimates, more scenarios of rain gauge density and combination need to be designed, and the sensitivity of precipitation merging estimates to rain gauge locations also needs to be investigated. Furthermore, the influence of the satellite-derived precipitation data with different qualities on the gauge-satellite merged precipitation estimates in different rain gauge density scenarios also needs to be explored. These issues would be critical for the improvement of precipitation spatial estimation and the optimization of rain gauge network.

The automatic weather observing network system of China has been established and gradually improved since 2006. There are nearly 40 000 national and regional automatic weather stations (AWSs) in 2015, and the observation network density has increased greatly especially in the eastern regions. This highly dense weather observing network provides superior data support for investigating the impacts of rain gauge configuration on multiplatform precipitation estimates. In this study, two provinces, Anhui and Hubei, in the middle and lower reaches of the Yangtze River of China with a high gauge network density are selected as the study area. The objectives of this study are to: 1) examine the influence of rain gauge density and spatial distribution on the gauge-satellite merged precipitation analysis at monthly and ten-day temporal scales, respectively and 2) analyze the influence of the satellite-derived precipitation data with different qualities on the gauge-satellite merged precipitation estimates in different rain gauge density scenarios. The remainder of this article is organized as follows. Section II describes the study area and the data sets; Section III is about the gauge-satellite precipitation merging scheme; the designs of rain gauge configuration and the rain gauge network optimization scheme are described; Section IV describes the results; the discussions and some possible future research proposals are given in Section V; and conclusion is drawn in Section VI.

II. STUDY AREA AND DATA

A. Study Area

The study area, Anhui and Hubei provinces of China, is between 29°01′–34°38′N and 108°21′–119°37′E and has an area of about 326 000 km² (Fig. 1). It lies in the south–north climate transition zone in China, with a subhumid warm temperate monsoon climate in the north of Huaihe River and a subtropical humid monsoon climate in the south of

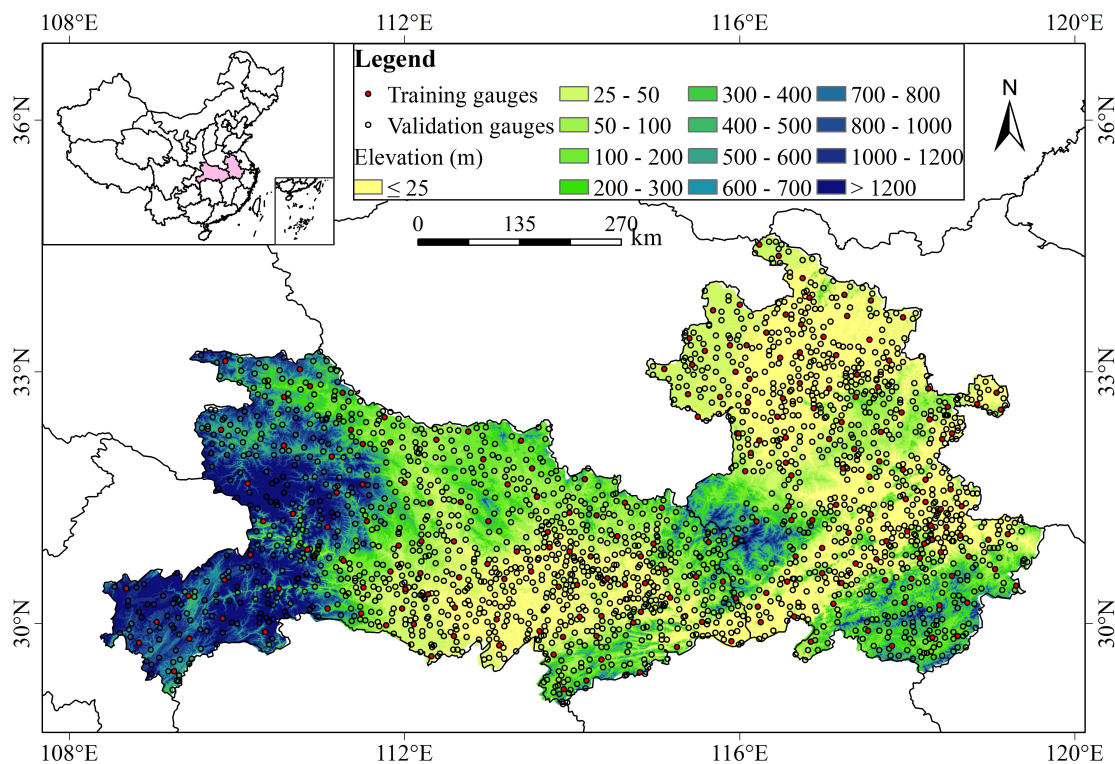


Fig. 1. Location and topography of the study area.

Huaihe River. The annual average precipitation varies between 700 and 1670 mm from north to south and concentrated mainly in the spring and summer. The abundant summer precipitation accounts for 40%–60% of the annual precipitation, while the winter precipitation accounts only for 4%–15%. The topography of this study area includes plains, hills, and mountains. The elevation ranges between 92 m below sea level and 3105 m above sea level: the high altitudes are mainly distributed in the western area of Hubei Province and the western and southern areas of Anhui Province.

B. Data

We use both the ground and satellite-based precipitation data in the precipitation merged estimation. Daily rain gauge data from 2204 AWSs with quality-control procedures over Anhui Province and Hubei Province ranging from 2010 to 2015 were used. The quality-control procedures include climatological and regional extreme value checks, temporal and spatial consistency check, and verification against mosaic radar reflectivity observations. The few missing daily records of some stations have been estimated using the surrounding observations and ordinary kriging. Each station covers about 148 km² on average (Fig. 1). Among them, 220 roughly evenly distributed rain gauges (about 10%, red points) are selected as validation stations using *k*-means clustering, and the remaining 1984 rain gauges (about 90%, unfilled points) are used for merging. The rain gauges in the western mountainous area of Anhui Province are sparser than the other areas. The ten-day and monthly rain gauge precipitation data were aggregated from daily AWSs data sets, respectively. For ten-day temporal scale, each month is divided into three periods, that is, Day

1–Day 10, Day 11–Day 20, and Day 21 to the last day of this month. The analysis is also conducted at the ten-day temporal scale because many crop drought and flood disasters are monitored at this scale in China.

The satellite-derived precipitation data used were generated from the Tropical Rainfall Measuring Mission (TRMM) [48] and the Global Precipitation Measurement (GPM) mission [49]. The TRMM was jointly conducted by the National Aeronautics and Space Administration (NASA) and the Japanese Aerospace Exploration Agency (JAXA) in 1997. The latest Version-7 daily TRMM Multisatellite Precipitation Analysis (TMPA) 3B42 product, which covers the global areas between 50°S and 50°N at 0.25° spatial resolution, is applied in this article. The recent 3B42 algorithm combines a number of satellite sensors and GPCP monthly rain-gauge analysis to produce the best precipitation estimates [5]. The Version 7 daily 3B42 precipitation data used in our study, covering 2010–2015, were obtained from the NASA archive (<https://pmm.nasa.gov/data-access/downloads/trmm>) and aggregated to ten-day and monthly values, respectively. The GPM, initiated by NASA and JAXA as a global successor to TRMM, is an international network of satellites. Its Core Observatory carrying the first space-borne Ku-/Ka-band Dual-frequency Precipitation Radar (DPR) and a multichannel GPM Microwave Imager (GMI) was launched on February 27, 2014. The Integrated Multi-satellitE Retrievals for GPM (IMERG) is designed to estimate precipitation from all passive-microwave instruments, infrared-based observations, and GPCP gauge rain-gauge analysis [49]. The Version 06 IMERG Final Run daily data sets with 0.1° spatial resolution from 2010 to

2015 are used in this study. Now, the extension of IMERG back to the TRMM era has been finished, and the complete record from June 2000 to present can be downloaded from the website <https://gpm.nasa.gov/data-access/downloads/gpm>. The TMPA 3B42 V7 is now decommissioned and has been replaced by the IMERG product which generates precipitation at finer scale than 3B42 and is more performant [50].

Considering the influence of the topographical factors on precipitation, a 90-m Digital Elevation Model (DEM) data from the Shuttle Radar Topography Mission (SRTM) are also used in this study. The SRTM 90 m DEM data were downloaded from the website (<https://srtm.csi.cgiar.org/>) and resampled to 1 km using pixel averaging.

III. METHODOLOGY

A. Downscaling-Integration Framework for Monthly and Ten-Day Precipitation Estimates

A two-stage downscaling-integration approach proposed by Chen *et al.* [23] is used to combine the satellite-derived precipitation data and rain gauge measurements to produce monthly and ten-day precipitation data sets at high spatial resolution (1 km \times 1 km). The approach has been proven to be an efficient alternative to combine different data to produce improved high-resolution precipitation estimates. Downscaling the high-resolution satellite precipitation before merging with ground observations can improve the merging performance [29]. In the downscaling-integration framework, the first step is to downscale the low-resolution satellite-derived precipitation to 1-km spatial resolution using area-to-point kriging (ATPK) for better matching ground observations. Then, the downscaled satellite precipitation data are merged with the rain gauge observations by applying the geographically weighted regression kriging (GWRK). Additional geographical factors (i.e., longitude, latitude, and elevation) are also involved in the merging model.

1) *ATPK for Downscaling Satellite-Derived Precipitation Data:* The ATPK is a geostatistical-based downscaling scheme that calculates the point values from areal information [51]–[53]. The principle of ATPK is similar to that of the ordinary kriging, that is, the target point value is the linear weighted sum of the neighboring areal data. The difference between them lies in the calculation of variances. The ordinary kriging uses the point-to-point covariances in the kriging system, while the ATPK uses the block-to-point and block-to-block covariances. Assuming an areal pixel value is the average values of all discretized point values within it, the block-to-point and block-to-block covariances can be expressed as regularized functions of point-to-point covariance. Under the assumption of second-order stationarity, the point-support covariance can be replaced by the point-support semivariogram, which is estimated by an iterative deconvolution procedure using the area-support data in the ATPK [54]. More details of the ATPK estimating equations, kriging system, and its calculating process can be found in [51] and [23].

The ATPK takes into account the sizes of the area-support data and their spatial correlations and also gives the accuracy estimation of downscaling. Kyriakidis [51] proved an

important property of ATPK, that is, the consistency property: the average of ATPK estimates within an area-support is equal to the original value of this area-support. This property enables ATPK to effectively preserve the important information in the original areal data [55]. An original satellite-based pixel value records the areal precipitation of this pixel. Because the target spatial resolution (1 km) of this study is much less than the original spatial resolution, the fine spatial resolution pixel value can be treated as the point value in the ATPK model. The downscaled satellite precipitation data using ATPK would be used as inputs in the next GWRK model.

2) *Gauge-Satellite Merged Precipitation Estimates Using GWRK:* The GWRK is a combination of GWRK and ordinary kriging. GWR is a spatial local regression algorithm that effectively considers the nonstationarity relationship between variables [56], [57]. Based on GWR, the variable y (e.g., precipitation) at spatial point i can be expressed as

$$y_i = \beta_0(\mu_i, v_i) + \sum_{k=1}^p \beta_k(\mu_i, v_i) x_{ik} + \varepsilon_i \quad (1)$$

where (μ_i, v_i) is the longitude and latitude coordinate of the i th spatial point; x_{ik} and ε_i are the value of the k th auxiliary variable and the regression residual at spatial point i , respectively; $\beta_k(\mu_i, v_i)$ is the regression coefficient of the k th auxiliary variable at spatial point i , which is calculated using weighted least squares estimation

$$\hat{\beta}(\mu_i, v_i) = (X^T W(\mu_i, v_i) X)^{-1} (X^T W(\mu_i, v_i) Y) \quad (2)$$

where X and Y are the vectors of the auxiliary and the dependent variables, respectively; $W(x)$ is the spatial weighting matrix. There are several available kernel functions, for example, fixed Gaussian, fixed bisquare, adaptive Gaussian, and adaptive bisquare to calculate the weighting matrix. In this study, the adaptive bisquare kernel function and cross-validation (CV) are used to calculate the weight and determine the optimal bandwidth, respectively [56], [58].

In this study, the downscaled satellite-based precipitation and related geographical factors (i.e., latitude, longitude, and elevation) are used as auxiliary variables and the gauge-based precipitation is used as the dependent variable to construct the GWRK merging model. In the GWRK model, the GWR is first applied to obtain the regression coefficients and residual of each observation point, and then the GWR precipitation estimates and the spatial kriged residuals using ordinary kriging are added to obtain the final GWRK precipitation estimates.

B. Rain Gauge Network Configurations

To investigate the impacts of different rain gauge configurations including the rain gauge network density and its spatial distribution on monthly and ten-day gauge-satellite merged precipitation estimates, 21 different rain gauge density levels (r) were defined, which are the ratios of the available rain gauges to the total training rain gauges. The number of rain gauges and the average controlling area per gauge for different percentages of total training rain gauges (1984) are shown in Table I. Only 50 rain gauges are present at the minimum rain

TABLE I
NUMBER OF RAIN GAUGES AND AVERAGE REPRESENTING AREA PER GAUGE (km²) IN DIFFERENT PERCENTAGES OF TOTAL RAIN GAUGES

Percentage of rain gauges (%)	2.5	5	8	10	15	20	25	30	35	40	45
Number of rain gauges	50	100	159	199	298	397	496	596	695	794	893
Average controlling area per gauge (km ²)	6520	3260	2050	1638	1094	821	657	547	469	411	365
Percentage of rain gauges (%)	50	55	60	65	70	75	80	85	90	95	100
Number of rain gauges	992	1092	1191	1290	1389	1488	1588	1687	1786	1885	1984
Average controlling area per gauge (km ²)	329	299	274	253	235	219	205	193	183	173	164

gauge network density, roughly 6520 km² representing area per rain gauge on average. The average area of each gauge is only about 164 km² when all 1984 training rain gauges are used.

To analyze the effects of the rain gauge network density on the gauge-satellite merged precipitation estimates, a roughly uniformly distributed rain gauge combination in the whole region for each rain gauge network density scenario is obtained using *k*-means clustering. Specifically: 1) the *k*-means clustering is first used to divide all training rain gauges (1984) to 50 categories, and then one station is randomly selected from each category to form a network configuration of 50 training stations in the 2.5% density scenario. If a selected station is closest to the validation station, a new station will be reselected randomly to ensure that the training station has a certain distance (more than 4 km) from the validation station; 2) similarly, using the *k*-means clustering to acquire 100 stations in the 5% rain gauge density scenario from all training stations. Calculating the spatial distances between these stations and the 50 stations obtained in the first step and removing the corresponding 50 stations that are closest to the reserved stations in the previous step from the 100 stations. Then, the remaining stations and the previous reserved 50 stations compose the network configuration of 100 training stations in the 5% density scenario; and 3) the other gauge network configurations in higher density scenarios (e.g., 8%, 10%, ..., and 95%) could be iteratively obtained as step. In this way, the numbers of stations at different gauge densities increases successively on the basis of the obtained 50 stations in the 2.5% rain gauge density scenario. This schema ensures that all the gauge stations at lower density levels can be selected at higher density levels and evenly distributed in the whole study area.

In addition, we also obtain 200 different network combinations for each gauge density scenario by randomly selecting rain gauges from the 1984 training rain gauges, to explore the effect of rain gauge configurations on the gauge-satellite merged precipitation estimates. This results in a total of 4201 (i.e., 21 × 200 plus the original training set of 1984 rain gauges) different rain gauge combinations for both monthly and ten-day precipitation estimates.

To evaluate the precipitation estimates of GWRK at different rain gauge densities, ground observations from 220 independent rain gauges are taken as references (as shown in Fig. 1). Three assessment indicators, that is, root-mean-square error (RMSE), relative bias (Bias), and coefficients of determination (R^2), are used.

C. Rain Gauge Network Optimization

For a limited set of rain gauges in a specific region, the problem of rain gauge network optimization can be formulated as finding gauge locations that provide optimal precipitation estimates. In principal, we could try all rain gauge combinations and identify the “best” network configuration for a given gauge density. However, the number of combinations would be tremendous for practical applications, which would need significant computational time and may cause “combination explosion” problem. The simulated annealing algorithm has been used to solve this kind of large-scale combinatorial optimization problem [59]–[61]. In this study, we use the spatial simulated annealing to optimize the gauge locations for gauge-satellite precipitation estimates for a given time.

Spatial simulated annealing is a commonly used combinatorial optimization algorithm [61]. It is an extension of the simulated annealing in which a series of new sampling combinations are generated. First, an arbitrary combination of samples is obtained. Then, the optimization is carried out iteratively, starting from this combination, by slightly and randomly shifting one station location in a random direction and distance. For each new candidate combination, the criterion value is calculated and compared with the criterion value of the previous combination. The improved combination is always accepted, while the worse combination is also accepted with some probability to avoid local optimum [61]. As the number of iterations increases, the probability of accepting a worse combination reduces. The procedure repeats itself until a fixed number of iterations have been completed, or new candidate combinations have no improvements for many times. In this study, the GWRK mean square error is taken as the objective function and the spatial simulated annealing procedure is stopped when 6000 iterations are completed.

IV. RESULTS

A. Precipitation Estimates Using ATPK and GWRK

High spatial resolution merged precipitation data at monthly and ten-day scales from 2010 to 2015 are generated by combining the ground-based observations of 1984 rain gauges with the satellite precipitation data and geographical ancillary data (i.e., longitude, latitude, and altitude data) using the two-stage downscaling-integration approach. In the following, the original TMPA and IMERG precipitation data are labeled as OTMPA and OIMERG, and the corresponding downscaled

TABLE II

AVERAGE STATISTICS FOR THE ORIGINAL SATELLITE PRODUCTS (OTMPA AND OIMERG) AND THEIR DOWNSCALED (DTMPA AND DIMERG) AND GWRK MERGED (DTMPA_GWRK AND DIMERG_GWRK) PRECIPITATION ESTIMATES FROM 2010 TO 2015 AT MONTHLY AND TEN-DAY TEMPORAL SCALES

	Monthly				Ten-day			
	RMSE (mm)	MAE (mm)	Bias (%)	R^2	RMSE	MAE	Bias (%)	R^2
OTMPA	38.84	29.16	11.29	0.511	23.85	17.33	30.85	0.320
OIMERG	34.44	26.52	16.55	0.603	20.66	15.28	35.20	0.414
DTMPA	37.92	28.61	11.37	0.533	22.87	16.75	29.96	0.346
DIMERG	34.19	26.09	16.56	0.607	20.43	15.13	34.17	0.423
DTMPA_GWRK	23.81	16.26	0.04	0.760	10.95	7.01	-0.20	0.738
DIMERG_GWRK	23.79	16.25	-0.02	0.760	11.00	6.95	-0.18	0.737

data are labeled as DTMPA and DIMERG, respectively. The GWRK merging results of DTMPA and DIMERG with rain gauge observations are labeled as DTMPA_GWRK and DIMERG_GWRK, respectively. Table II presents the average statistics of the original satellite products and their down-scaled and GWRK merged precipitation estimates for all months and ten days from 2010 to 2015 compared with rain gauge observations. Fig. 2 shows the evaluation of the down-scaled satellite precipitation data (DTMPA and DIMERG) and GWRK merged precipitation data (DTMPA_GWRK and DIMERG_GWRK) from 2010 to 2015 at the monthly scale (left) and ten-day scale (right) using 220 independent verification stations' data. Table II shows that the IMERG-based precipitation data have an improved statistical performance compared with the TMPA-based precipitation data, and the down-scaled satellite precipitation data have slightly better performance than their original satellite data with smaller RMSE and MAE values and better R^2 values both at monthly and ten-day temporal scales. Like the original satellite data, the down-scaled satellite precipitation data still have some overestimation in the study area. The overestimation for low precipitation level in IMERG product is much higher than that in the TMPA product, resulting in its average Bias value larger than that of the TMPA product.

As can be seen from Table II and Fig. 2, both monthly and ten-day GWRK merged precipitation data show significantly improved performance than the down-scaled satellite precipitation data set. Although DIMERG has better statistical performance than DTMPA, their GWRK merging results with all rain gauge observations show similar evaluation index values both at monthly and ten-day scales over the study area. The RMSE and MAE values of the monthly precipitation data for both satellite-based and merged precipitation data are higher than that of the ten-day precipitation data, and summer has higher RMSE and MAE values than winter. This is mainly because the precipitation amount is larger at the monthly scale than that at the ten-day scale or larger in summer than that in winter. It is noted that some ten-day satellite precipitation data, for example, the first ten days of November 2010, the second ten days of February 2011, the last ten days of January 2014, and the second ten days of October 2015, even have more than 100% Bias values. This

could be attributed to the little precipitation at these times, in which a small deviation value of the satellite precipitation data may produce a large relative bias value. For example, the average precipitation of gauge observations and DTMPA precipitation data over the study area in the second ten days of January 2010 are 1.33 and 3.83 mm, respectively. Their deviation value is 2.5 mm, while their relative bias value is 187.97%. In terms of R^2 , the merged monthly precipitation data show higher spatial consistency with rain gauge observations than that of the merged ten-day precipitation data.

Fig. 3 shows the spatial distribution of the original satellite-derived precipitation data (i.e., TMPA and IMERG), down-scaled satellite precipitation (i.e., DTMPA and DIMERG), and GWRK merged precipitation data (i.e., DTMPA_GWRK and DIMERG_GWRK) using all rain gauges' data for June 2015 and the first ten days of July 2014, respectively. It can be observed that TMPA and IMERG have similar spatial distribution for both June 2015 and the first ten days of July 2014. The down-scaled TMPA and IMERG precipitation data produced by ATPK preserve the spatial information well in the original satellite precipitation data. There is a large spatial difference between the original satellite-derived precipitation data and the GWRK merged precipitation data in June 2015. The heavy precipitation in the original satellite precipitation data is mainly distributed in the southeast of Anhui Province, while the heavy precipitation events in the GWRK merged precipitation data are mainly distributed in the central and southwestern regions, and the merged heavy precipitation obviously covers less area than that in the satellite-derived precipitation data. The spatial maps for the first ten days of July 2014 show that the satellite product presents similar spatial pattern as the GWRK merged precipitation data. However, the satellite product overestimates the magnitude of the precipitation events in the northern regions and underestimates the magnitude of heavy precipitation events in the southern regions of Anhui Province. Overall, the GWRK merged precipitation data for both June 2015 and first ten days of July 2014 not only have improved accuracy but also can more effectively reflect precipitation spatial details and heterogeneity than the satellite precipitation data.

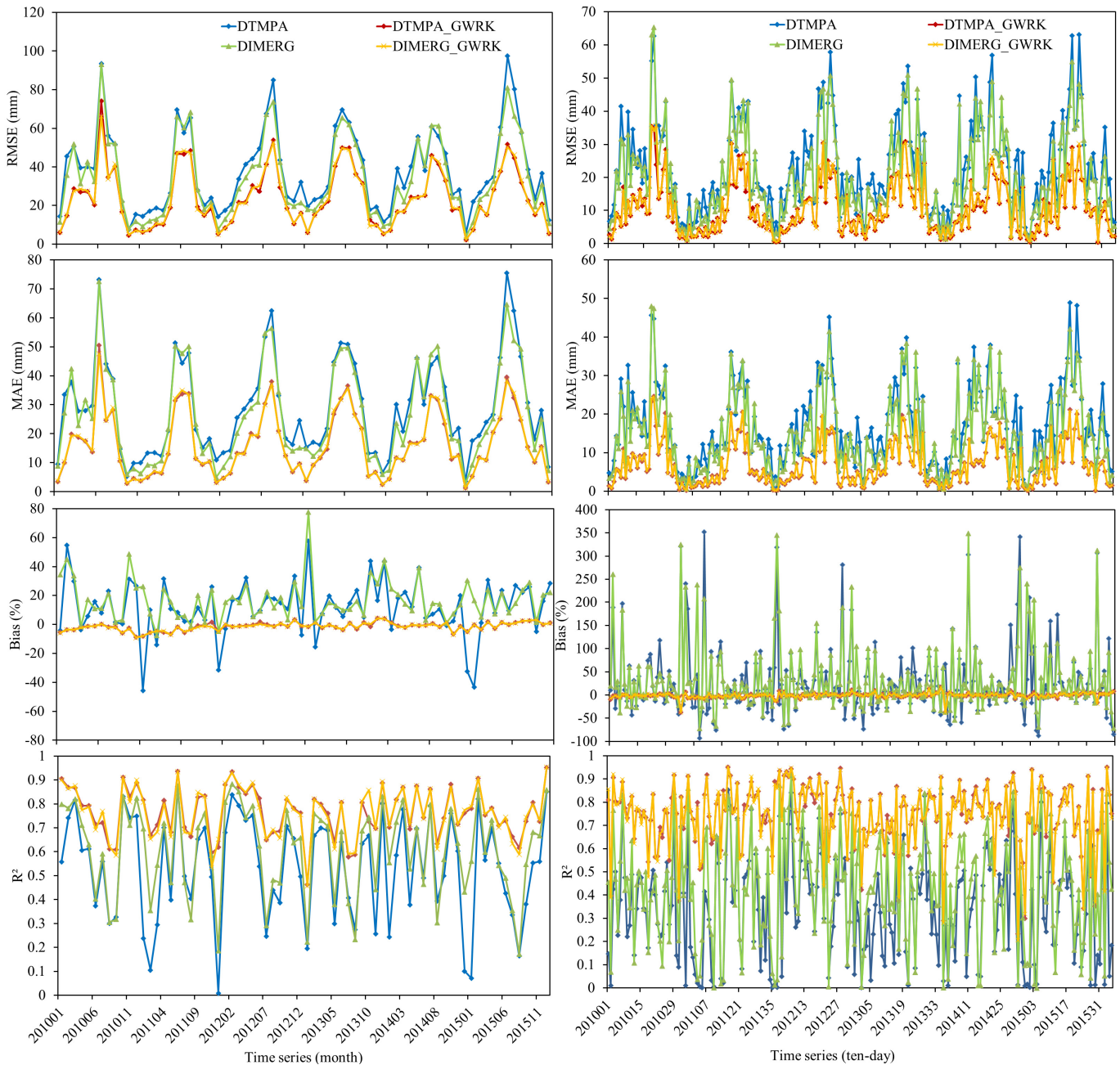


Fig. 2. Evaluation of the downscaled TRMM precipitation data (DTMPA and DIMERG) and GWRK merged precipitation data (DTMPA_GWRK and DIMERG_GWRK) from 2010 to 2015 on (Left) monthly scale and (Right) ten-day scale.

B. Precipitation Estimates Based on Different Rain Gauge Network Configuration Using GWRK

Fig. 4 shows the average error statistics of the GWRK merged monthly and ten-day precipitation data from 2010 to 2015 for different rain gauge network densities. It can be seen that the RMSE value of the merged results gradually decreases, and the R^2 value gradually increases and then level off with the increased rain gauge network density. When the gauge network density is low, the RMSE and R^2 values vary more than that at the high network density; the Bias values of the merged results are close to zero at different gauge densities and are slightly larger at low gauge densities. The merged monthly

precipitation data have higher R^2 values in all different rain gauge network densities than that of the ten-day precipitation data. As shown in Table I, it is obvious that the merged monthly and ten-day precipitation estimates using GWRK at all different rain gauge network densities have better performance than the downscaled monthly and ten-day satellite precipitation data. DIMERG_GWRK has better statistical performance than that of DTMPA_GWRK in terms of RMSE and R^2 values when the gauge network density is low, while their performances are similar at high gauge network densities.

As described in Section III-B, we also obtain 200 different rain gauge network combinations for each gauge density scenario by randomly selecting rain gauges from the 1984 rain

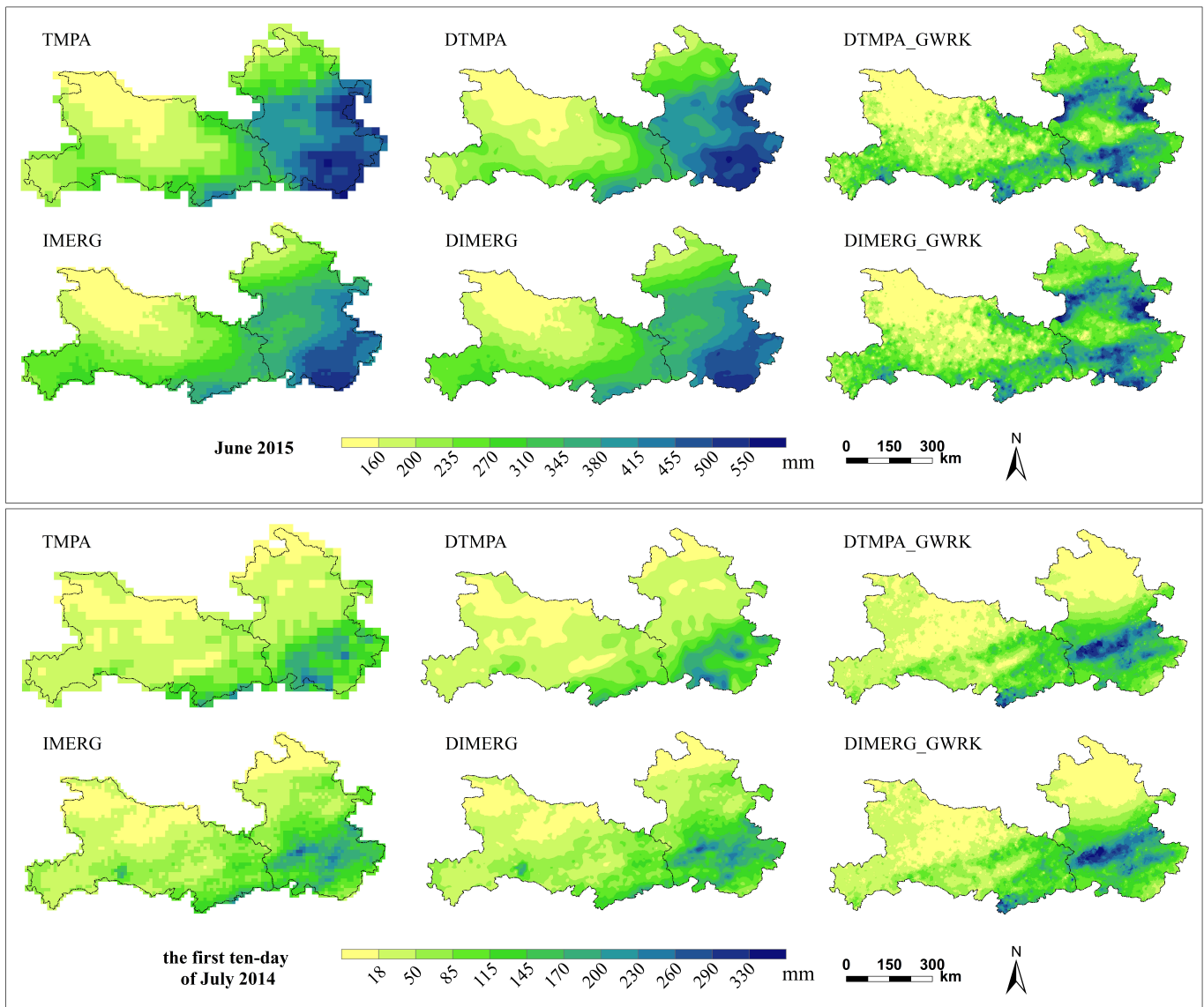


Fig. 3. Spatial distribution of the original satellite-derived precipitation data [(Left) TMPA and IMERG], the downscaled satellite precipitation data [(Middle) DTMPA and DIMERG], and the GWRK merged precipitation data [(Right) DTMPA_GWRK and DIMERG_GWRK] for June 2015 and the first ten days of July 2014, respectively. Precipitation estimates based on different rain gauge network configuration using GWRK.

gauges, to examine the influence of the rain gauge configurations on precipitation spatial estimation. Fig. 5 shows the average statistics of the GWRK merged monthly and ten-day precipitation in the study area from 2010 to 2015 at different rain gauge network densities. The RMSE values decrease and the R^2 values increase for both the merged monthly and ten-day precipitation data, and both gradually tend to be stable with the increased rain gauge network density. In the low gauge density scenarios, the Bias values of the merged results using different gauge combinations show relatively larger fluctuation than that in higher gauge density scenarios, but are all within $\pm 10\%$, and the fluctuations of the Bias values for monthly gauge-satellite precipitation estimates are less than the ten-day merged precipitation data. The results of both the monthly and ten-day gauge-satellite precipitation estimates derived by different spatial rain gauge combinations

all exhibit certain fluctuations. On the whole, the results at the low gauge network densities have greater fluctuations than that of the high densities. This indicates that the influence of the gauge spatial distribution on the GWRK merged results at low rain gauge network densities is greater than that at high rain gauge network density. The gauge-satellite precipitation estimates using GWRK may generate more accurate spatial precipitation estimates than slightly increasing the rain gauge network density, if the rain gauge spatial distribution is appropriate. On the average, the gaps of RMSE and R^2 values between DTMPA_GWRK and DIMERG_GWRK decrease with the increase in the rain gauge network density. When the rain gauge network is sparse, DIMERG_GWRK is significantly better than DTMPA_GWRK, while when the rain gauge network is dense, their performances are similar.

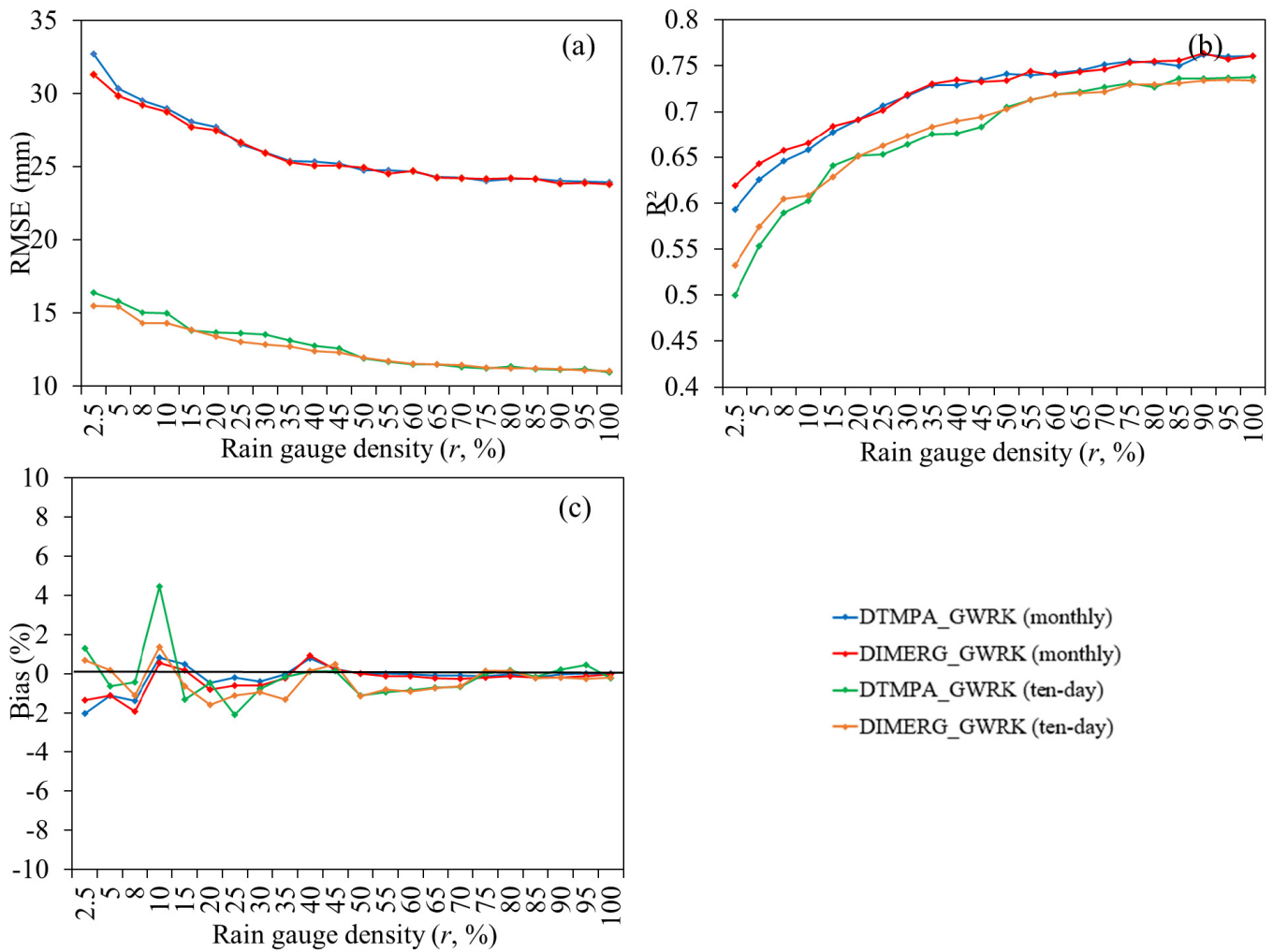


Fig. 4. Average statistics. (a) RMSE, (b) R^2 , and (c) Bias of the GWRK merged monthly and ten-day precipitation data from 2010 to 2015 for different rain gauge network densities.

We compare the R^2 values of the monthly and ten-day precipitation data for dry (winter) and wet (summer) seasons at different rain gauge network densities in Fig. 6. It can be seen that the gauge-satellite merged precipitation estimates in the dry season have higher R^2 values than that in the wet season at all different gauge network densities, while the variations in R^2 are larger in the wet season than that of the dry season as the rain gauge network density increases both at monthly and ten-day scales. In the dry season, most of the monthly and ten-day merged results show improved performance compared with DTMPA and DIMERG at the 2.5% rain gauge density. Most R^2 values of the monthly and ten-day merged results in the dry season using 200 different gauge combinations are above 0.66 and 0.50, respectively. The average R^2 values of DTMPA and DIMERG are 0.49 and 0.66 at the monthly scale and 0.23 and 0.38 at the ten-day scale, respectively. In the dry season, DIMERG_GWRK shows better statistical performance than DTMPA_GWRK at the monthly scale in the low gauge density scenarios, while it performs better than DTMPA_GWRK at the ten-day scale in all gauge density scenarios. The R^2 values of the merged monthly precipitation

data increase slightly with the increase in the gauge network density and level off when the network density reaches 30%. There is a larger range for the ten-day precipitation merged results with the rain-gauge configuration changing than that for the monthly precipitation merged results, and the change in the R^2 values tends to be stable when the gauge density reaches 50%. In the dry season, the zero precipitation values of most rain gauges at some times is an important factor affecting the performance of the GWRK merged ten-day precipitation, which makes it difficult to solve the GWRK model parameters, and consequently the merged effect is not good.

In the wet season, the R^2 values of the GWRK merged monthly and ten-day precipitation data both vary greatly as the rain-gauge configuration changes. They gradually stabilize when the gauge network density reaches 60%, and the statistics of the monthly merged results are better than that of the ten-day merged results, but the fluctuation is larger than that of the ten-day merged results. The R^2 values of the DTMPA and DIMERG precipitation data are similar, that is, 0.45 and 0.46, at the monthly scale and 0.38 and 0.39 at the ten-day scale, respectively. DTMPA_GWRK and DIMERG_GWRK at

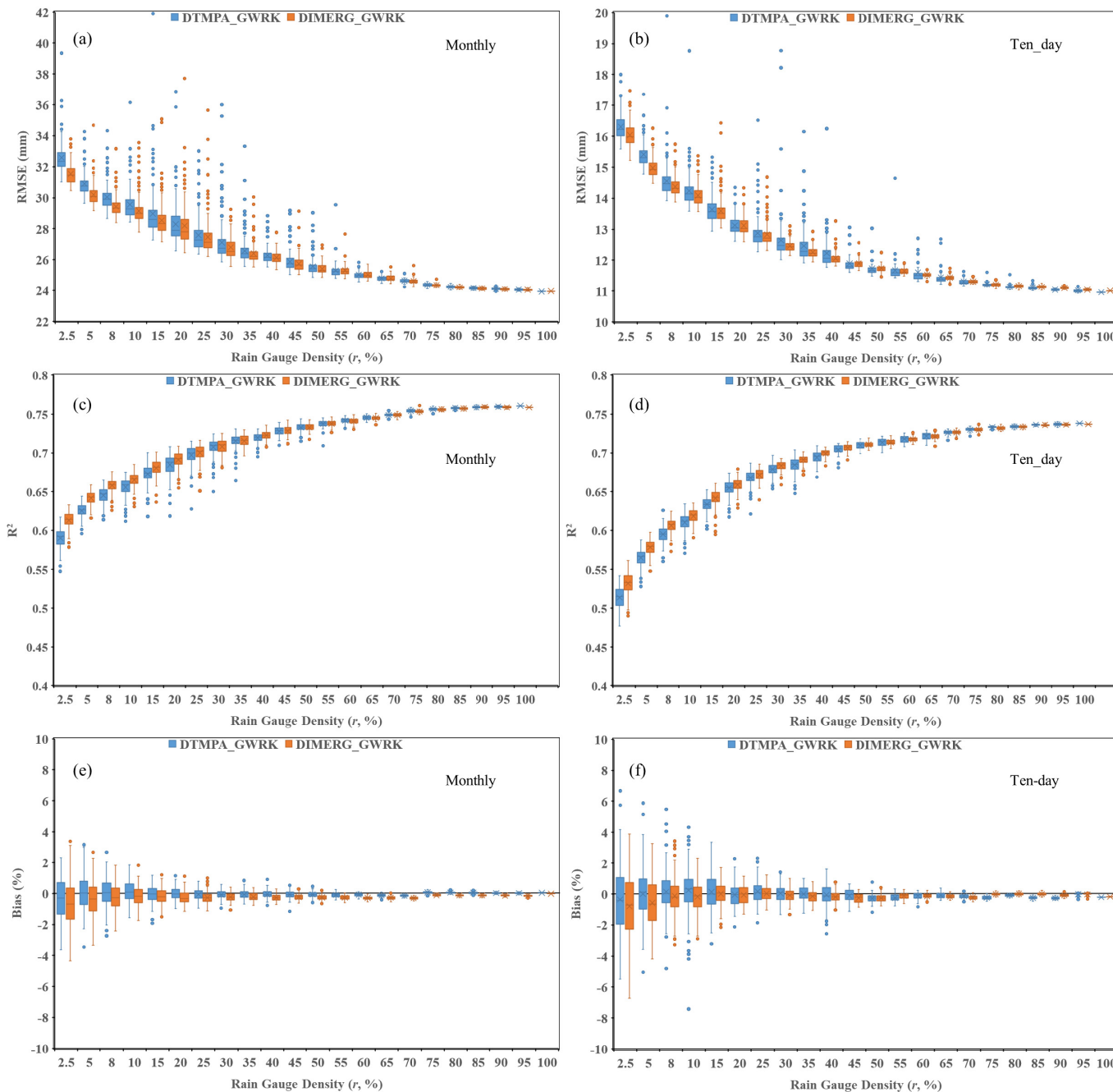


Fig. 5. Box plots of the average statistics. (a) and (b) RMSE, (c) and (d) R^2 , and (e) and (f) Bias of (Left) GWRK merged monthly and (Right) ten-day precipitation (DTMPA_GWRK and DIMERG_GWRK) from 2014 to 2015 at different rain gauge network densities.

all gauge network densities perform better than DTMPA and DIMERG; their average R^2 values of the 200 monthly merged results are 0.51 and 0.52 and are 0.45 and 0.46 for the ten-day merged results at the 2.5% rain gauge density, respectively. As the rain gauge density increases, DTMPA_GWRK performs better than DIMERG_GWRK in the wet season. One of the reasons for this is that DIMERG_GWRK exhibits less improvements than DTMPA_GWRK with the increase in rain gauge density some times, such as the last ten days of June 2010 and the second ten days of June 2011.

The precipitation calculations at unsampled locations are usually influenced by the neighboring gauges. Here, we use the monthly and ten-day precipitation merged results with 200 rain gauge combinations at the 2.5% rain gauge network density to analyze the influence of the distance between the target pixel and its nearest gauge (Fig. 7). Theoretically, there should be 44 000 (220×200) samples, and the largest distance between the target pixel and its nearest neighboring gauge is 326 km. After removing samples at some specific ranges, the sample size of which is less than 30, the actual total sample size is 43 126 and the largest distance is 141 km.

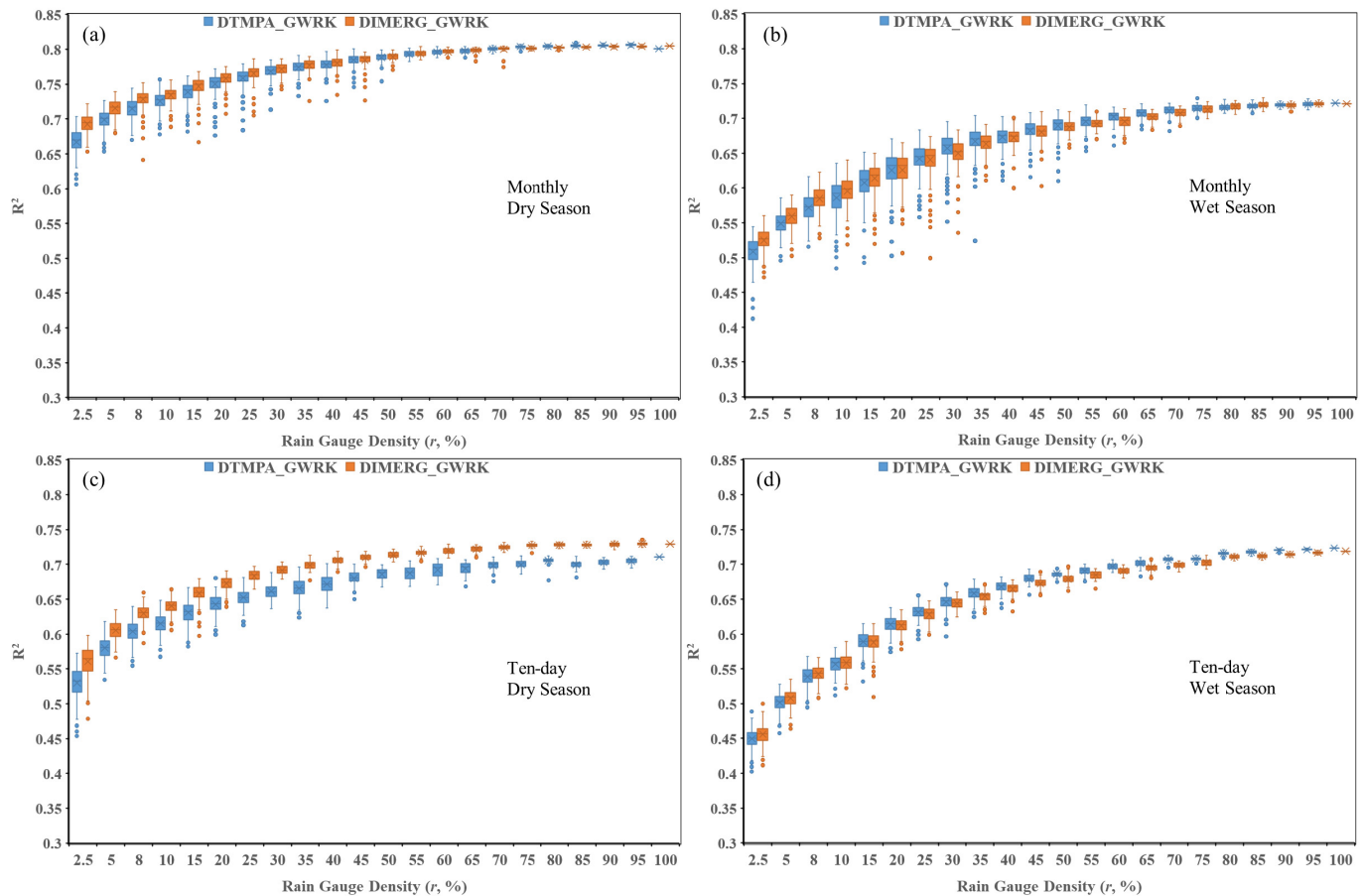


Fig. 6. The R^2 values of the (a) and (b) monthly and (c) and (d) ten-day precipitation estimates generated by GWRK for dry (winter, left) and wet (summer, right) seasons at different rain gauge network densities.

As shown in Fig. 7, the assessment indicator values of both the downscaled satellite-based and merged precipitation data fluctuate greatly when the sample size is small. The RMSE decreases, while R^2 increases as the target pixel gets close to its nearest gauge for both the monthly and ten-day precipitation data, and the gap between DTMPA_GWRK and DIMERG_GWRK decreases simultaneously. When the distance between the target pixel and its nearest gauge is large, the statistical performance of DIMERG_GWRK is significantly better than that of DTMPA_GWRK, which is consistent with the results in Figs. 4 and 5. For the monthly merged results, when the distance between the target pixel and its nearest gauge is within about 70 km, the DTMPA_GWRK results perform better than that of DTMPA. For the ten-day merged results, DTMPA_GWRK show better statistical values than the DTMPA data, within 100 km between the target pixel and its nearest gauge. It means that compared with DTMPA, DTMPA_GWRK is more effective for monthly and ten-day precipitation estimates if the distance between the target pixel and its nearest gauge is within about 70 and 100 km, respectively. DIMERG_GWRK performs better than DIMERG both for the monthly and ten-day precipitation estimates if the distance between the target pixel and its nearest gauge is within about 60 and 85 km, respectively. It should be noted that the distance, 85 km, of the GWRK for the ten-day precipitation data is larger than that of the

monthly precipitation estimates. It might be attributed to that the monthly satellite precipitation data are more consistent with ground observations than the ten-day satellite data.

C. Optimal Gauge Spatial Distribution for Precipitation Estimates

Three different optimized gauge combinations are obtained using the spatial simulated annealing for June 2015 and the first ten-day of July 2014, respectively. Fig. 8 shows that the variances of the prediction error steadily decrease and level off with the increase in the iteration number. During these initial phases, the smaller the number of rain gauges used in precipitation estimation, the larger the fluctuation of the prediction indicator values both for June 2015 and the first ten days of July 2014. A slight variation in the rain gauge location may cause a large change in the precipitation spatial estimation when the rain gauges are sparsely distributed.

Fig. 9 shows the initial and optimized rain gauge networks of different numbers of rain gauges (i.e., 50, 159, and 496) and their corresponding precipitation distributions of the DIMERG_GWRK results for June 2015 and early July 2014, respectively. The rain gauge spatial location could have a great effect on the GWRK precipitation estimates. It is obvious that the GWRK merged results with the optimized rain gauges' data perform much better than the ones with

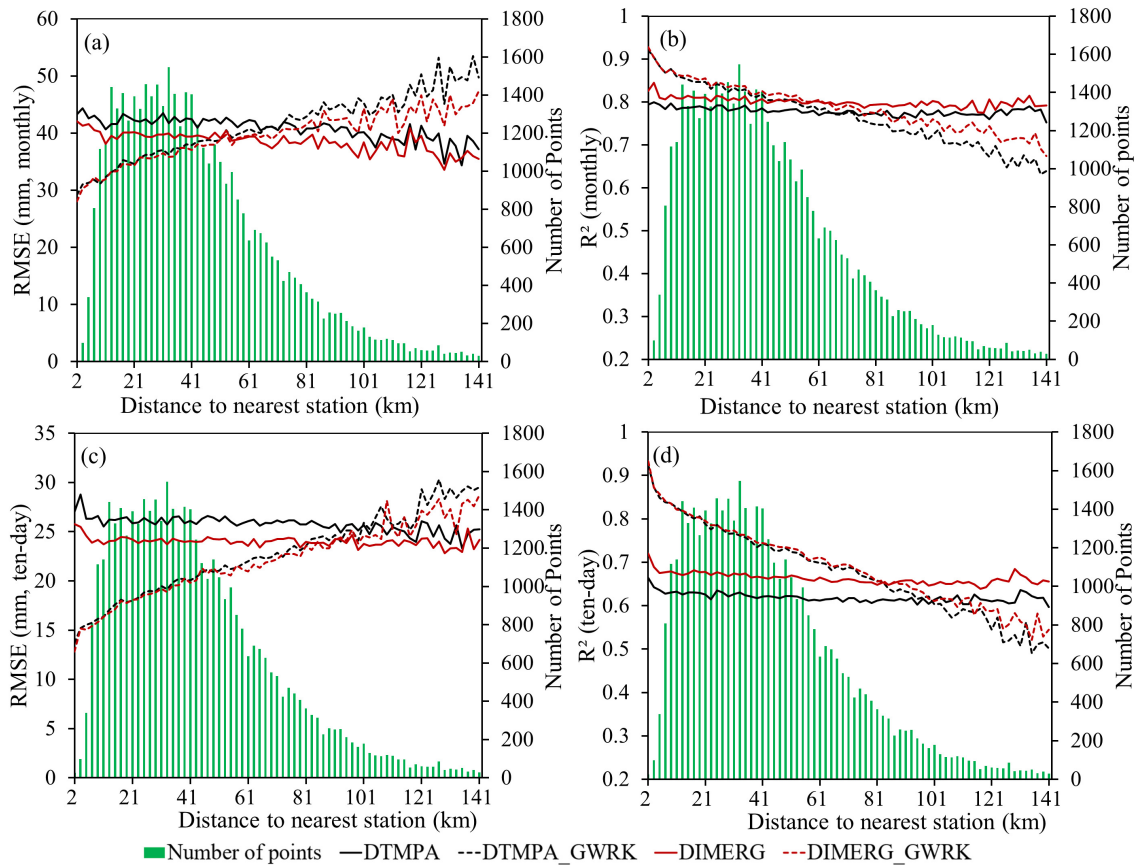


Fig. 7. (a) and (c) RMSE and (b) and (d) R^2 values of the monthly and ten-day precipitation estimates generated by GWRK as a function of distance to the nearest gauge.

random rain gauge network designs for the sparse rain gauge network. The optimized rain gauges by simulated annealing for June 2015 and the first ten days of July 2014 are different due to their different precipitation spatial distribution characteristics. But they are more uniformly distributed over the study area than the initial rain gauges by random sampling. Comparing the GWRK merged results of these optimized rain gauge configurations at the three rain-gauge densities, it can be observed that the more the rain gauges, the better the merged assessments and the finer the precipitation spatial distribution, both for June 2015 and the first ten days of July 2014.

Fig. 9 reveals that the fewer rain gauges available, the greater the role of the rain gauge locations have in the gauge-satellite merged precipitation estimates. For instance, comparable precipitation estimates (RMSE = 21.98 mm and $R^2 = 0.91$) could be produced using the optimized 159 rain gauges with that using all rain gauges in the first ten days of July 2014. Although the precipitation estimate created using the 50 optimized rain gauge network [Fig. 9(b)] is not as good as the one using all rain gauges in June 2015, it is still much better than the scenario in which the initial 50 rain gauges are used [Fig. 9(a)].

The effective representativeness of rain gauges depends on the precipitation field structure and may have great influence on the gauge-satellite merged precipitation estimates. Taking the initial and optimized rain gauge networks with different

numbers of rain gauges, that is, 50, 159, and 496, as example, the semivariograms of the precipitation observations for June 2015 and the first ten days of July 2014 are analyzed, respectively (Fig. 10). Compared with the case where the initial rain gauge networks with the same density are used, the semivariogram curves originated from the optimized rain gauge networks are closer to the semivariogram curve using all rain gauges. For example, the semivariogram curve of the optimized 496 rain gauges is the closest, the case where all rain gauges were used, while it is opposite if the initial 50 rain gauges are used for both June 2015 and the first ten days of July 2014. Different semivariogram parameters (i.e., nugget, sill, and range) in two different times suggest that they have different spatial structure characteristics of precipitation. A higher nugget in June 2015 indicates that there is higher variability than the early first ten days of July 2014, which will affect the gauge-satellite precipitation estimation. At the same gauge network density, the gauge-satellite merging estimation with large spatial heterogeneity of precipitation structure has higher uncertainty than that with small spatial heterogeneity of precipitation.

V. DISCUSSION

This study explores the impacts of rain gauge network density and spatial distribution on combined gauge-satellite precipitation estimates. Rain gauge observation is an

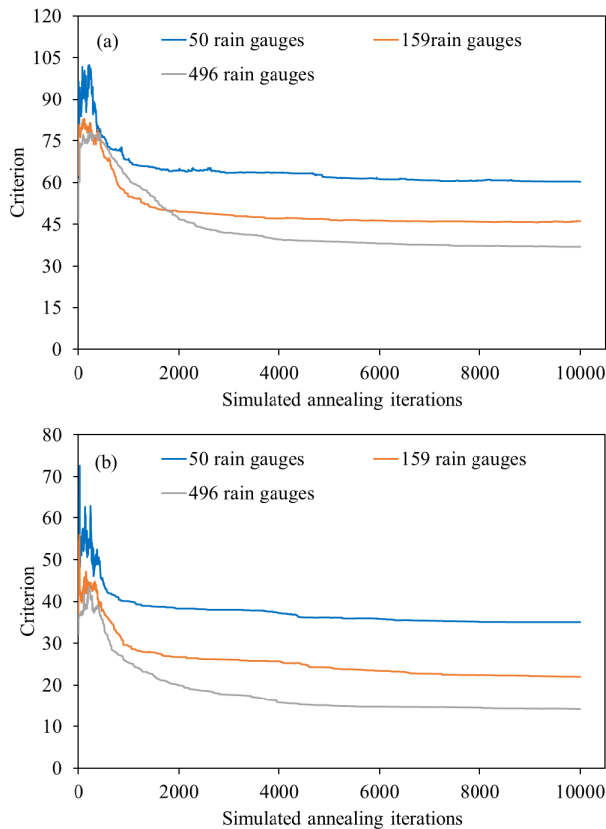


Fig. 8. Traces of the minimization criterion with increasing simulated annealing iterations for (a) June 2015 and (b) first ten days of July 2014. The three cases are with 50 (blue), 159 (orange), and 496 (gray) rain gauges, respectively.

important input data source in gauge-satellite merging precipitation estimation, and the density and spatial distribution of the rain gauge network greatly affects the precipitation estimation. Generally, the performance of gauge-satellite precipitation merged results by GWRK increases and gradually levels off with increasing rain gauge network density (Fig. 4). There are also cases where the rain gauge network density increases but the performance of the merged results remains the same or slightly decrease. For instance, the ten-day DTMPA_GWRK merged results at 75% rain gauge density have a slightly better performance than the merged results at 80% density in terms of RMSE and R^2 statistics. If the precipitation information obtained by some stations cannot reflect the overall precipitation situation within a certain spatial range of the region or is significantly different from that of other surrounding observation stations, increasing the observations of these stations in the gauge-satellite merged precipitation estimates may reduce their precipitation spatial estimation performance. It should be noted that the rain gauge network density scenarios in Fig. 4 are designed ensuring the higher gauge density scenarios always contain all rain gauges of the last lower density scenario and maintaining a roughly even distribution of the used rain gauges. If the rain gauges increase randomly, the deterioration of precipitation estimates may become more pronounced as rain gauges increase.

In the study area, when the rain gauge density continues to decrease from 20% (i.e., an average density of about 821 km²

per rain gauge), the capacity of combining the gauge-satellite precipitation data to estimate the spatial distribution of precipitation decreases rapidly; while the performance of the gauge-satellite precipitation estimation tends to stabilize when the rain gauge density is about larger than 50%, that is, about 329 km² per rain gauge (Fig. 5). Similar results can still be obtained when we use shorter period (e.g., 2013–2015) than that of this study to analyze in the study area, but the evaluation statistical values (i.e., RMSE, R^2 , and Bias) and the variation range of the statistical values from different rain gauge combinations at a certain density are different. Actually, the necessary rain gauge density largely depends on practical requirements, precipitation spatial heterogeneity, and regional characteristics. WMO [62] established the minimum rain gauge density guidelines for different climatic and geographic zones, in which the recommended minimum densities of nonrecording stations at mountains and interior plains are 250 and 575 km² per station, respectively. Mountainous areas with higher precipitation spatial variability have more recommended stations. The errors of the gauge-satellite merging estimation could also be significantly reduced by optimizing the rain gauge distribution. An appropriate rain gauge combination could produce higher accurate merged results than that using a slightly higher rain gauge density. The spatial location of rain gauges also has a great effect on the gauge-satellite precipitation estimates. The lower the rain gauge network density, the greater the influence of rain gauge locations on precipitation estimates. This indicates that great uncertainty originated from rain gauge combinations might exist in gauge-satellite precipitation merging estimation if available rain gauges are limited. Optimizing the rain gauge locations to improve the rain gauge representativeness is critical for gauge-satellite precipitation estimation especially in areas with sparse rain gauges. Overall, optimizing the rain gauge combination has a greater impact on precipitation estimates than increasing a few numbers of rain gauges when the rain gauge network density is low. Although different optimal rain gauge configurations are observed for different precipitation spatial distributions at different times (Fig. 9), better gauge-satellite merged precipitation estimates could be obtained using a more evenly distributed rain gauge network (Figs. 4 and 5). Similar findings were also reported by Xu *et al.* [46] and Lopez *et al.* [47]. In addition, Antil *et al.* [63] pointed out that better gauge-based mean areal rainfall estimation could be achieved using reasonable rain gauge combinations than that using all available rain gauges; Zeng *et al.* [64] suggested that additional rain gauges should be installed in mountains with more orographic rain. It should be noted that the gauge-satellite merging algorithm and the sampling optimization algorithm are not the focus of this study. The results of this study emphasize the benefits of appropriate rain gauge network configuration including density and distribution and improved satellite-derived precipitation data to gauge-satellite merged precipitation estimates.

The rain gauge network density and spatial distribution also greatly affects the precipitation interpolation estimation only using the rain gauge data. Manz *et al.* [65] showed that the kriging-based precipitation estimation using only

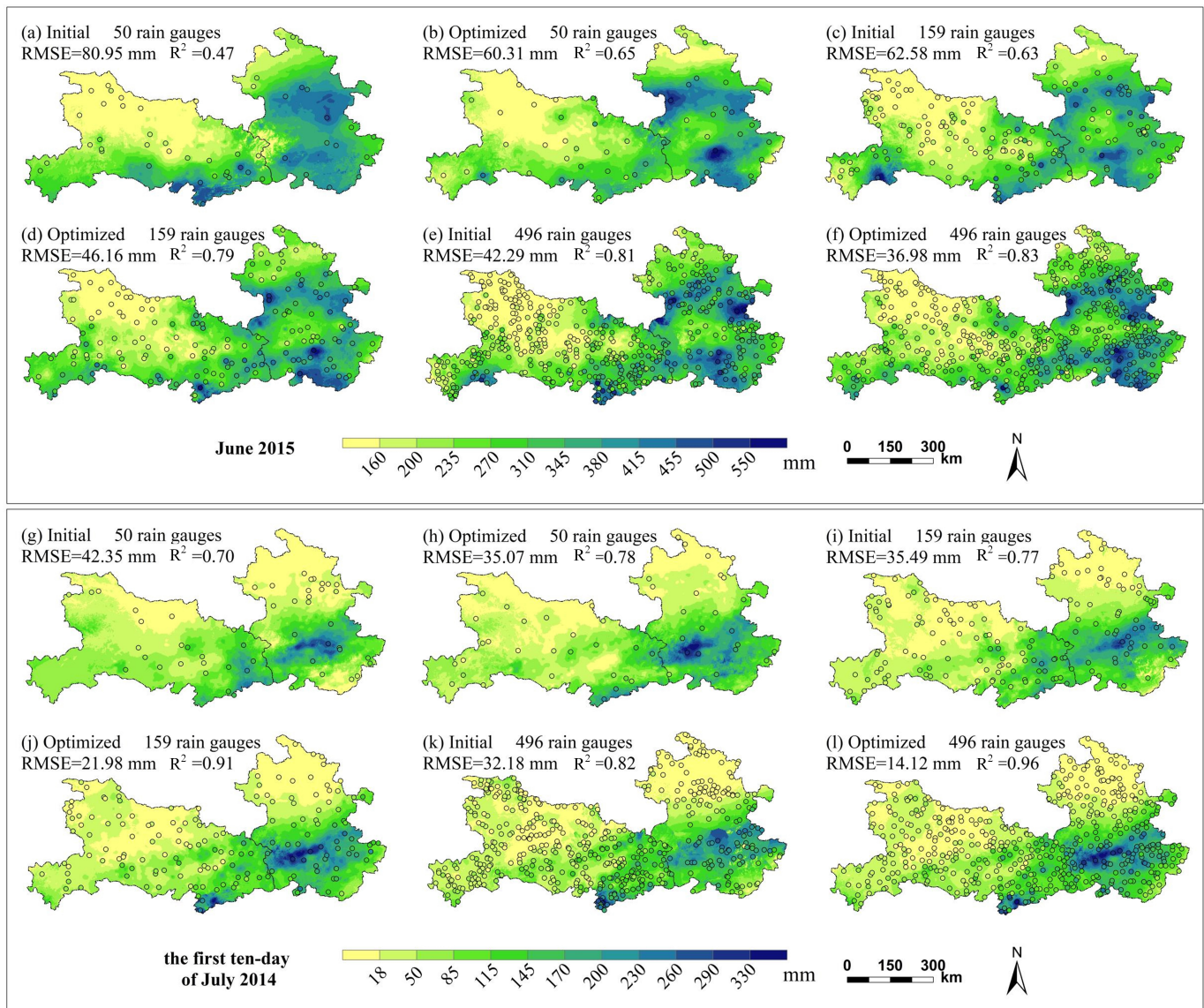


Fig. 9. Initial and optimized rain gauge networks with different numbers of rain gauges (i.e., 50, 159, and 496) and their corresponding precipitation spatial distribution of the DIMERG_GWRK results for June 2015 and the first ten days of July 2014. (a) Initial 50 rain gauges, RMSE = 80.95 mm, $R^2 = 0.47$. (b) Optimized 50 rain gauges, RMSE = 60.31 mm, $R^2 = 0.65$. (c) Initial 159 rain gauges, RMSE = 62.58 mm, $R^2 = 0.63$. (d) Optimized 159 rain gauges, RMSE = 46.16 mm, $R^2 = 0.79$. (e) Initial 496 gauges, RMSE = 42.29 mm, $R^2 = 0.81$. (f) Optimized 496 rain gauges, RMSE = 36.98 mm, $R^2 = 0.83$. (g) Initial 50 rain gauges, RMSE = 42.35 mm, $R^2 = 0.70$. (h) Optimized 50 rain gauges, RMSE = 35.07 mm, $R^2 = 0.78$. (i) Initial 159 rain gauges, RMSE = 35.49 mm, $R^2 = 0.77$. (j) Optimized 159 rain gauges, RMSE = 21.98 mm, $R^2 = 0.91$. (k) Initial 496 rain gauges, RMSE = 32.18 mm, $R^2 = 0.82$. (l) Optimized 496 rain gauges, RMSE = 14.12 mm, $R^2 = 0.96$.

rain gauge observations had a higher dependence on gauge density than the gauge-satellite combined precipitation estimation, and its performance showed a consistent deterioration with decreasing network density. Park *et al.* [42] indicated that the RMSE statistics of ordinary kriging precipitation interpolation results increased with the available rain gauges decreased, and the ordinary kriging method could produce comparable precipitation spatial estimates with multivariate kriging merging algorithms when large rain gauges were used. Lopez *et al.* [47] indicated that a decrease in localized rain gauges at high altitudes with high precipitation magnitudes and variability could significantly reduce the ability of spatial interpolation to precipitation estimation. In our previous

work [23], we also observed that the ordinary kriging method produced precipitation spatial estimates with greater errors than these geographical-based merging schemes in the rain gauge sparse areas, and the ordinary kriging-based precipitation estimates in some locations of these areas even showed lower accuracy than the satellite-derived precipitation estimates.

DIMERG_GWRK performs better than DTMPA_GWRK in the low gauge density scenarios, but the gap decreases as the rain gauge network density increases (Fig. 5). It implies that the influence of the satellite-derived precipitation data on the gauge-satellite merged precipitation estimates decreases with the increase in the rain gauge network density. In areas where

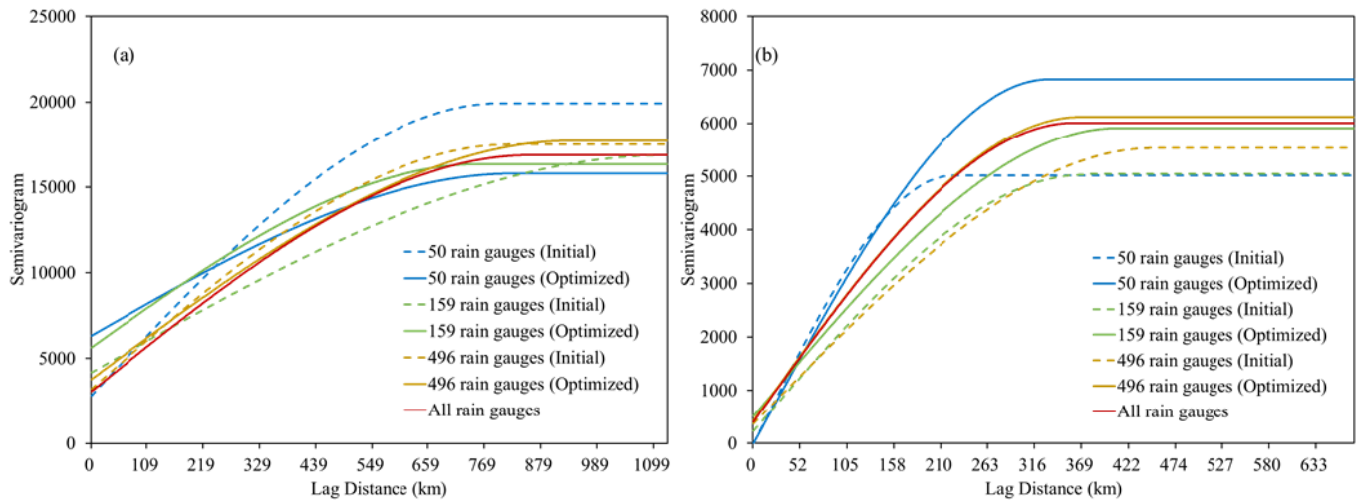


Fig. 10. Semivariograms of ground precipitation observations of the initial and optimized rain gauge networks for (a) June 2015 and (b) first ten days of July 2014. The rain gauge numbers are 50, 159, and 496 respectively.

the rain gauges are sparse, the improved satellite data cannot only provide effective supplement for ground observations but also improve the performance of the gauge-satellite merging estimation. The TMPA 3B42 V7 and the Version 06 IMERG Final Run products used in this study have been rescaled using the GPCP gauge-based reanalysis. It could be inferred that if uncalibrated satellite data are applied in the gauge-satellite merged precipitation estimates, the merged results may be worse than DIMERG_GWRK and DTMPA_GWRK in the low gauge density scenarios. Different from the results in Fig. 5, DIMERG_GWRK performs better than DTMPA_GWRK at the ten-day scale in all gauge density scenarios in the dry season (Fig. 6). This result is greatly affected by some special results. For example, the R^2 values of DIMERG and DIMERG_GWRK are 0.53 and 0.76, respectively, while the R^2 values of DTMPA and the DIMERG_GWRK are 0.01 and 0.51, respectively, at the 45% rain gauge density. When removing these few results with large difference, the difference variation between DTMPA_GWRK and DIMERG_GWRK in Fig. 6 as the gauge density increases is similar to Fig. 5.

The improvement of the gauge-satellite merged precipitation estimates is still unsatisfactory at some times, for example, July 2013, mid-November 2014, and mid-August 2015. It is because the gauge-satellite merging estimation is influenced not only by the rain gauge density and location but also by the merging algorithm, uncertainty of input data, and precipitation spatiotemporal variability. It should be noted that the local regression prediction of GWRK may produce negative or unreasonable extreme precipitation values at locations where the environment variables have high variabilities. In this study, these prediction outliers are few in the precipitation merged results and are replaced with the average of the nearest eight neighboring values. The performance of the gauge-satellite precipitation merging estimation is positively correlated with the accuracy of the satellite precipitation data and is negatively correlated with precipitation spatial heterogeneity [23]. Furthermore, rain gauge network density and its spatial distribution are found to have a stronger influence

on the gauge-satellite merged precipitation estimates in the wet season than that in the dry season in this study (Fig. 6), which is partly due to the greater precipitation variability in the wet season. The wet season has abundant rainfall and more topographic rain in the study area. There is a large precipitation spatiotemporal variability in the wet season, where it leads to a large precipitation differences over small distances. The uncertainty of the gauge-satellite precipitation estimates using GWRK or other local estimation schemes would be large if spatial structures and variability of precipitation could not be well-characterized by limited ground-based measurements.

The results of this study can provide some useful guidelines for better precipitation estimation with multi-source data at different network densities. Although the analysis of this study is done for a specific basin, it is expected that the general conclusions about the impacts of rain gauge network configurations and satellite-derived data quality on the gauge-satellite precipitation estimation would also be applicable in other basins. But the characteristics, for example, the variation ranges and the threshold of rain gauge density when gauge-satellite merging tends to be stable, would vary with basins, which are closely related to the spatial heterogeneity of precipitation and the satellite-derived data quality in different climatic or topographic regions. Because the local climatology conditions the performance of satellite estimates and the spatial covariance of the precipitation fields. The precipitation variance is strongly scale-dependent and a robust gauge network needs to be able to capture variabilities across many hydrological scales, including the diurnal [66] and individual storm scales, especially in complex terrain. The impacts of rain gauge density and distribution on the gauge-satellite merged precipitation estimates at microtemporal scales needs to be further explored. Delrieu *et al.* [35] demonstrated that the radar had clear added value with respect to the rain gauge network for the shortest scales. We believe that it is possible to use deep learning methods to integrate more multi-source data such as radar-based precipitation data, cloud parameter data, and numerical model analysis data to obtain more precipitation spatial details.

In this article, this data-driven approach analyzed the impact of rain gauge configurations on precipitation estimation only from the perspective of data. In the real design of a regional station network, not only the representativeness of the stations for monitoring precipitation but also the economic, population, technological, and environmental conditions should be considered. In addition to meeting scientific needs, hydrological data collection sites can also be established to help water managers cope with extreme events such as floods or droughts and distribute water supplies in competing uses. There are usually more observation sites in densely populated and economically developed areas than in sparsely populated areas. In further studies, it would be interesting to investigate the influence of more diversified climate on the gauge-satellite precipitation estimates, including the effectiveness of the algorithms at shorter temporal scales, for example, daily and hourly. The geographical-model-based schemes, for example, kriging with external drift, universal cokriging, and stratified block kriging, are of particular values to optimize the rain gauge network and provide quantitative guidelines for practical rain gauge network design [67]–[69]. In addition, the impacts of the long-time precipitation data should also be evaluated in the optimization of rain gauge network configuration.

VI. CONCLUSION

This study examines the impacts of rain gauge network density and its spatial distribution on the gauge-satellite merged precipitation estimates at monthly and ten-day temporal scales. Two provinces in the middle and lower reaches of the Yangtze River of China with a high rain gauge network density in eastern China are selected as the study area. A two-stage downscaling-integration approach is applied in the gauge-satellite precipitation estimation from 2010 to 2015. Various scenarios of rain gauge density and combination are designed and their corresponding merged precipitation estimates are evaluated using statistical indices. The gauge-satellite merged results (i.e., DTMPA_GWRK and DIMERG_GWRK) using the TMPA 3B42 V7 product and the Version 06 IMERG Final Run product, respectively, are compared at monthly and ten-day temporal scales. Three different optimized gauge combinations at three different rain gauge densities are obtained using the spatial simulated annealing for June 2015 and the first ten days of July 2014, respectively. In addition, the influence of the distance between the location and its nearest gauge on gauge-satellite merged precipitation estimates is also analyzed. The results show that: first, the influence of rain gauge network configuration including density and distribution on the gauge-satellite merged precipitation estimates gradually decreases with the increase in rain gauge density. When the gauge density reaches a certain threshold, the statistical performance of the gauge-satellite merged estimates tends to be stable. The gauge-satellite merged precipitation estimates are more sensitive to the rain gauge network density in the wet season and at ten-day temporal scale than in the dry season and monthly temporal scale, respectively, which have lower R^2 values and larger variability with the increase in rain gauge density. Second, generally, DIMERG_GWRK has better statistical performance

than DTMPA_GWRK in the low gauge density scenarios, and their gaps decrease as the rain gauge network density increases. In areas with sparse rain gauges, improving the quality of the satellite precipitation data would be beneficial for the gauge-satellite merging estimation. Third, overall, the rain gauge spatial distribution is found to play a greater role for the correction of gauge-satellite precipitation estimation than a slight increase in the rain gauge network density. Good performance of the combined gauge-satellite precipitation estimation can be achieved by optimizing the rain gauge network. Better gauge-satellite precipitation merging estimates could be obtained using a more evenly distributed rain gauge network. It should be noted that the quality of the gauge-satellite merged precipitation estimates using geographical local calibration method (e.g., GWRK) may be lower than that of the original satellite-derived precipitation data if the rain gauges are too sparse.

ACKNOWLEDGMENT

The authors would like to thank the Anhui Meteorological Information Centre (AMIC), Hefei, China, for providing the rain gauge data. They would also like to thank the National Aeronautics and Space Administration (NASA), Washington, D.C., USA, for providing the satellite and DEM data sets free of charge. The valuable comments and advice by anonymous peer reviewers are also well-appreciated.

REFERENCES

- [1] C.-Y. Xu, L. Tunemar, Y. D. Chen, and V. P. Singh, "Evaluation of seasonal and spatial variations of lumped water balance model sensitivity to precipitation data errors," *J. Hydrol.*, vol. 324, nos. 1–4, pp. 80–93, Jun. 2006.
- [2] R. Celleri, P. Willems, W. Buytaert, and J. Feyen, "Space-time rainfall variability in the Paute basin, Ecuadorian Andes," *Hydrol. Processes*, vol. 21, no. 24, pp. 3316–3327, Nov. 2007.
- [3] K.-L. Hsu, X. Gao, S. Sorooshian, and H. V. Gupta, "Precipitation estimation from remotely sensed information using artificial neural networks," *J. Appl. Meteorol.*, vol. 36, no. 9, pp. 1176–1190, Sep. 1997.
- [4] G. J. Huffman *et al.*, "The global precipitation climatology project (GPCP) combined precipitation dataset," *Bull. Amer. Meteorol. Soc.*, vol. 78, no. 1, pp. 5–20, Jan. 1997.
- [5] G. J. Huffman *et al.*, "The TRMM multisatellite precipitation analysis (TMPA): Quasi-global, multiyear, combined-sensor precipitation estimates at fine scales," *J. Hydrometeorol.*, vol. 8, no. 1, pp. 38–55, Feb. 2007.
- [6] T. Kubota *et al.*, "Global precipitation map using satellite-borne microwave radiometers by the GSMaP project: Production and validation," *IEEE Trans. Geosci. Remote Sens.*, vol. 45, no. 7, pp. 2259–2275, Jul. 2007.
- [7] A. Ochoa, L. Pineda, P. Crespo, and P. Willems, "Evaluation of TRMM 3B42 precipitation estimates and WRF retrospective precipitation simulation over the Pacific-Andean region of Ecuador and Peru," *Hydrol. Earth Syst. Sci.*, vol. 18, no. 8, pp. 3179–3193, Aug. 2014.
- [8] S. Sorooshian, K.-L. Hsu, X. Gao, H. V. Gupta, B. Imam, and D. Braithwaite, "Evaluation of PERSIANN system satellite-based estimates of tropical rainfall," *Bull. Amer. Meteorol. Soc.*, vol. 81, no. 9, pp. 2035–2046, Sep. 2000.
- [9] S. K. Adhikary, A. G. Yilmaz, and N. Muttill, "Optimal design of rain gauge network in the middle Yarra river catchment, Australia," *Hydrol. Processes*, vol. 29, no. 11, pp. 2582–2599, May 2015.
- [10] A. Aghakouchak, A. Behrangi, S. Sorooshian, K. Hsu, and E. Amitai, "Evaluation of satellite-retrieved extreme precipitation rates across the central United States," *J. Geophys. Res., Atmos.*, vol. 116, no. D2, Jun. 2011, Art. no. D02115.
- [11] A. S. Gebregiorgis and F. Hossain, "Estimation of satellite rainfall error variance using readily available geophysical features," *IEEE Trans. Geosci. Remote Sens.*, vol. 52, no. 1, pp. 288–304, Jan. 2014.

- [12] V. Maggioni, E. I. Nikolopoulos, E. N. Anagnostou, and M. Borga, "Modeling satellite precipitation errors over mountainous terrain: The influence of gauge density, seasonality, and temporal resolution," *IEEE Trans. Geosci. Remote Sens.*, vol. 55, no. 7, pp. 4130–4140, Jul. 2017.
- [13] P. Xie and P. A. Arkin, "Global precipitation: A 17-year monthly analysis based on gauge observations, satellite estimates, and numerical model outputs," *Bull. Amer. Meteorol. Soc.*, vol. 78, no. 11, pp. 2539–2558, Nov. 1997.
- [14] R. F. Adler *et al.*, "The version-2 global precipitation climatology project (GPCP) monthly precipitation analysis (1979–present)," *J. Hydrometeorol.*, vol. 4, no. 6, pp. 1147–1167, Dec. 2003.
- [15] G. J. Huffman *et al.*, "Global precipitation at one-degree daily resolution from multisatellite observations," *J. Hydrometeorol.*, vol. 2, no. 1, pp. 36–50, Feb. 2001.
- [16] S. Curtis, A. Salahuddin, R. F. Adler, G. J. Huffman, G. Gu, and Y. Hong, "Precipitation extremes estimated by GPCP and TRMM: ENSO relationships," *J. Hydrometeorol.*, vol. 8, no. 4, pp. 678–689, Aug. 2007.
- [17] K. E. Dayem, D. C. Noone, and P. Molnar, "Tropical western Pacific warm pool and maritime continent precipitation rates and their contrasting relationships with the Walker Circulation," *J. Geophys. Res., Atmos.*, vol. 112, no. D6, Mar. 2007, Art. no. D06101.
- [18] R. Fensholt and K. Rasmussen, "Analysis of trends in the Sahelian 'rain-use efficiency' using GIMMS NDVI, RFE and GPCP rainfall data," *Remote Sens. Environ.*, vol. 115, no. 2, pp. 438–451, Feb. 2011.
- [19] A. Yatagai, T. N. Krishnamurti, V. Kumar, A. K. Mishra, and A. Simon, "Use of APHRODITE rain gauge-based precipitation and TRMM 3B43 products for improving Asian monsoon seasonal precipitation forecasts by the superensemble method," *J. Climate*, vol. 27, no. 3, pp. 1062–1069, Feb. 2014.
- [20] D. Nerini *et al.*, "A comparative analysis of TRMM–rain gauge data merging techniques at the daily time scale for distributed rainfall–runoff modeling applications," *J. Hydrometeorol.*, vol. 16, no. 5, pp. 2153–2168, Oct. 2015.
- [21] J. McPhee and S. A. Margulis, "Validation and error characterization of the GPCP-1DD precipitation product over the contiguous United States," *J. Hydrometeorol.*, vol. 6, no. 4, pp. 441–459, Aug. 2005.
- [22] D. Zheng and W. G. M. Bastiaanssen, "First results from version 7 TRMM 3B43 precipitation product in combination with a new downscaling–calibration procedure," *Remote Sens. Environ.*, vol. 131, pp. 1–13, Apr. 2013.
- [23] Y. Chen *et al.*, "A new downscaling–integration framework for high-resolution monthly precipitation estimates: Combining rain gauge observations, satellite-derived precipitation data and geographical ancillary data," *Remote Sens. Environ.*, vol. 214, pp. 154–172, Sep. 2018.
- [24] F. I. Boushaki, K.-L. Hsu, S. Sorooshian, G.-H. Park, S. Mahani, and W. Shi, "Bias adjustment of satellite precipitation estimation using ground-based measurement: A case study evaluation over the southwestern United States," *J. Hydrometeorol.*, vol. 10, no. 5, pp. 1231–1242, Oct. 2009.
- [25] J. R. Rozante, D. S. Moreira, L. G. G. de Goncalves, and D. A. Vila, "Combining TRMM and surface observations of precipitation: Technique and validation over South America," *Weather Forecasting*, vol. 25, no. 3, pp. 885–894, Jun. 2010.
- [26] P. Xie and A.-Y. Xiong, "A conceptual model for constructing high-resolution gauge–satellite merged precipitation analyses," *J. Geophys. Res., Atmos.*, vol. 116, no. D21, Nov. 2011.
- [27] Y. Shen, P. Zhao, Y. Pan, and J. Yu, "A high spatiotemporal gauge–satellite merged precipitation analysis over China," *J. Geophys. Res., Atmos.*, vol. 119, no. 6, pp. 3063–3075, Mar. 2014.
- [28] S. Sinclair and G. Pegram, "Combining radar and rain gauge rainfall estimates using conditional merging," *Atmos. Sci. Lett.*, vol. 6, no. 1, pp. 19–22, Jan. 2005.
- [29] M. Li and Q. Shao, "An improved statistical approach to merge satellite rainfall estimates and raingauge data," *J. Hydrol.*, vol. 385, nos. 1–4, pp. 51–64, May 2010.
- [30] Z. Yang *et al.*, "Merging high-resolution satellite-based precipitation fields and point-scale rain gauge measurements—A case study in Chile," *J. Geophys. Res. Atmos.*, vol. 122, no. 10, pp. 5267–5284, May 2017.
- [31] A. Verdin, C. Funk, B. Rajagopalan, and W. Kleiber, "Kriging and local polynomial methods for blending satellite-derived and gauge precipitation estimates to support hydrologic early warning systems," *IEEE Trans. Geosci. Remote Sens.*, vol. 54, no. 5, pp. 2552–2562, May 2016.
- [32] B. Jongjin, P. Jongmin, R. Dongryeol, and C. Minha, "Geospatial blending to improve spatial mapping of precipitation with high spatial resolution by merging satellite-based and ground-based data," *Hydrol. Processes*, vol. 30, no. 16, pp. 2789–2803, Jul. 2016.
- [33] S. Xu, C. Wu, L. Wang, A. Gonsamo, Y. Shen, and Z. Niu, "A new satellite-based monthly precipitation downscaling algorithm with non-stationary relationship between precipitation and land surface characteristics," *Remote Sens. Environ.*, vol. 162, pp. 119–140, Jun. 2015.
- [34] Y. Tang, X. Yang, W. Zhang, and G. Zhang, "Radar and rain gauge merging-based precipitation estimation via geographical–temporal attention continuous conditional random field," *IEEE Trans. Geosci. Remote Sens.*, vol. 56, no. 9, pp. 5558–5571, Sep. 2018.
- [35] G. Delrieu, A. Wijnbrans, B. Boudevillain, D. Faure, L. Bonnifait, and P. E. Kirstetter, "Geostatistical radar–raingauge merging: A novel method for the quantification of rain estimation accuracy," *Adv. Water Resour.*, vol. 71, pp. 110–124, Sep. 2014.
- [36] E. Todini, "A Bayesian technique for conditioning radar precipitation estimates to rain-gauge measurements," *Hydrol. Earth Syst. Sci.*, vol. 5, no. 2, pp. 187–199, Jun. 2001.
- [37] A. Verdin, B. Rajagopalan, W. Kleiber, and C. Funk, "A Bayesian kriging approach for blending satellite and ground precipitation observations," *Water Resour. Res.*, vol. 51, no. 2, pp. 908–921, Feb. 2015.
- [38] B. Jin, Y. Wu, B. Miao, X. L. Wang, and P. Guo, "Bayesian spatiotemporal modeling for blending *in situ* observations with satellite precipitation estimates," *J. Geophys. Res., Atmos.*, vol. 119, no. 4, pp. 1806–1819, Feb. 2014.
- [39] S. Wang and X. Liang, "A parameter estimation framework for multi-scale Kalman smoother algorithm in precipitation data fusion," *Water Resour. Res.*, vol. 50, no. 11, pp. 8675–8693, Nov. 2014.
- [40] I. P. Gorenburg, D. McLaughlin, and D. Entekhabi, "Scale-recursive assimilation of precipitation data," *Adv. Water Resour.*, vol. 24, nos. 9–10, pp. 941–953, Nov. 2001.
- [41] R. Gupta, V. Venugopal, and E. Foufoula-Georgiou, "A methodology for merging multisensor precipitation estimates based on expectation-maximization and scale-recursive estimation," *J. Geophys. Res., Atmos.*, vol. 111, no. D2, pp. 93–108, Jan. 2006.
- [42] N.-W. Park, P. Kyriakidis, and S. Hong, "Geostatistical integration of coarse resolution satellite precipitation products and rain gauge data to map precipitation at fine spatial resolutions," *Remote Sens.*, vol. 9, no. 3, p. 255, Mar. 2017.
- [43] G. Bastin, B. Lorent, C. Duqué, and M. Gevers, "Optimal estimation of the average areal rainfall and optimal selection of rain gauge locations," *Water Resour. Res.*, vol. 20, no. 4, pp. 463–470, Apr. 1984.
- [44] C. Berndt, E. Rabiei, and U. Haberlandt, "Geostatistical merging of rain gauge and radar data for high temporal resolutions and various station density scenarios," *J. Hydrol.*, vol. 508, pp. 88–101, Jan. 2014.
- [45] A. Sthilair, T. B. M. J. Ouarda, M. Lachance, B. Bobée, J. Gaudet, and C. Gignac, "Assessment of the impact of meteorological network density on the estimation of basin precipitation and runoff: A case study," *Hydrol. Processes*, vol. 17, no. 18, pp. 3561–3580, Dec. 2003.
- [46] H. Xu, C.-Y. Xu, H. Chen, Z. Zhang, and L. Li, "Assessing the influence of rain gauge density and distribution on hydrological model performance in a humid region of China," *J. Hydrol.*, vol. 505, pp. 1–12, Nov. 2013.
- [47] M. Girons Lopez, H. Wennerström, L. Nordén, and J. Seibert, "Location and density of rain gauges for the estimation of spatial varying precipitation," *Geografiska Annaler: A, Phys. Geography*, vol. 97, no. 1, pp. 167–179, Mar. 2015.
- [48] J. Simpson, R. F. Adler, and G. R. North, "A proposed tropical rainfall measuring mission (TRMM) satellite," *Bull. Amer. Meteorol. Soc.*, vol. 69, no. 3, pp. 19–36, Mar. 1988.
- [49] A. Y. Hou *et al.*, "The global precipitation measurement mission," *Bull. Amer. Meteorol. Soc.*, vol. 95, pp. 701–722, May 2014.
- [50] A. S. Gebregiorgis *et al.*, "To what extent is the day 1 GPM IMERG satellite precipitation estimate improved as compared to TRMM TMPA-RT?" *J. Geophys. Res., Atmos.*, vol. 123, no. 3, pp. 1694–1707, Feb. 2018.
- [51] P. C. Kyriakidis, "A geostatistical framework for area-to-point spatial interpolation," *Geographical Anal.*, vol. 36, no. 3, pp. 259–289, Nov. 2004.
- [52] Q. Wang, W. Shi, and P. M. Atkinson, "Area-to-point regression kriging for pan-sharpening," *ISPRS J. Photogramm. Remote Sens.*, vol. 114, pp. 151–165, Apr. 2016.
- [53] P. C. Kyriakidis and E.-H. Yoo, "Geostatistical prediction and simulation of point values from areal data," *Geographical Anal.*, vol. 37, no. 2, pp. 124–151, Apr. 2005.

- [54] P. Goovaerts, "Kriging and semivariogram deconvolution in the presence of irregular geographical units," *Math. Geosci.*, vol. 40, no. 1, pp. 101–128, Jan. 2008.
- [55] Q. Wang, W. Shi, P. M. Atkinson, and Y. Zhao, "Downscaling MODIS images with area-to-point regression kriging," *Remote Sens. Environ.*, vol. 166, pp. 191–204, Sep. 2015.
- [56] G. M. Foody, "Geographical weighting as a further refinement to regression modelling: An example focused on the NDVI–rainfall relationship," *Remote Sens. Environ.*, vol. 88, no. 3, pp. 283–293, Dec. 2003.
- [57] S.-B. Duan and Z.-L. Li, "Spatial downscaling of MODIS land surface temperatures using geographically weighted regression: Case study in Northern China," *IEEE Trans. Geosci. Remote Sens.*, vol. 54, no. 11, pp. 6458–6469, Nov. 2016.
- [58] A. S. Fotheringham, C. Brunson, and M. Charlton, *Geographically Weighted Regression: The Analysis of Spatially Varying Relationships*. New York, NY, USA: Wiley, 2002.
- [59] J. W. Groenigen and A. Stein, "Constrained optimization of spatial sampling using continuous simulated annealing," *J. Environ. Qual.*, vol. 27, no. 5, pp. 1078–1086, Sep. 1998.
- [60] S. Galle and J. D. Creutin, "Ground network optimization using satellite information: Application to the French heliographic network," *IEEE Trans. Geosci. Remote Sens.*, vol. 27, no. 4, pp. 459–462, Jul. 1989.
- [61] G. B. M. Heuvelink, Z. Jiang, S. De Bruin, and C. J. W. Twenhöfel, "Optimization of mobile radioactivity monitoring networks," *Int. J. Geographical Inf. Sci.*, vol. 24, no. 3, pp. 365–382, Mar. 2010.
- [62] WMO, *Guide to Hydrological Practices Hydrology-From Measurement to Hydrological Information*, vol. 1, 6th ed. Geneva, Switzerland: WMO Technical Publication, 2008.
- [63] F. Anctil, N. Lauzon, V. Andréassian, L. Oudin, and C. Perrin, "Improvement of rainfall-runoff forecasts through mean areal rainfall optimization," *J. Hydrol.*, vol. 328, nos. 3–4, pp. 717–725, Sep. 2006.
- [64] Q. Zeng *et al.*, "The effect of rain gauge density and distribution on runoff simulation using a lumped hydrological modelling approach," *J. Hydrol.*, vol. 563, pp. 106–122, Aug. 2018.
- [65] B. Manz, W. Buytaert, Z. Zulkafli, W. Lavado, B. Willems, and L. A. Robles, "High-resolution satellite-gauge merged precipitation climatologies of the Tropical Andes," *J. Geophys. Res., Atmos.*, vol. 121, no. 3, pp. 1190–1207, Feb. 2016.
- [66] O. Sungmin and P. E. Kirstetter, "Evaluation of diurnal variation of GPM IMERG-derived summer precipitation over the contiguous US using MRMS data," *Quart. J. Roy. Meteorol. Soc.*, vol. 144, pp. 270–281, Jan. 2018.
- [67] J. Wang, Y. Ge, G. B. M. Heuvelink, and C. Zhou, "Spatial sampling design for estimating regional GPP with spatial heterogeneities," *IEEE Geosci. Remote Sens. Lett.*, vol. 11, no. 2, pp. 539–543, Feb. 2014.
- [68] Y. Ge, J. H. Wang, G. B. M. Heuvelink, R. Jin, X. Li, and J. F. Wang, "Sampling design optimization of a wireless sensor network for monitoring ecohydrological processes in the Babao river basin, China," *Int. J. Geographical Inf. Sci.*, vol. 29, no. 1, pp. 92–110, Jan. 2015.
- [69] A. M. J.-C. Wadoux, D. J. Brus, M. A. Rico-Ramirez, and G. B. M. Heuvelink, "Sampling design optimisation for rainfall prediction using a non-stationary geostatistical model," *Adv. Water Resour.*, vol. 107, pp. 126–138, Sep. 2017.



Yuanyuan Chen received the B.Sc. degree in geography information system from Northwest Agriculture and Forest University, Xianyang, China, in 2013, and the Ph.D. degree in applied remote sensing from Zhejiang University, Hangzhou, China, in 2018.

She is a Lecturer with the School of Information Management of Artificial Intelligence, Zhejiang University of Finance and Economics, Hangzhou. Her research interests include remote sensing of environment, spatial downscaling algorithms, and multisource data fusion techniques.



Jingfeng Huang was born in Zhangpu County, Zhangzhou, Fujian, China, in 1963. He received the B.S. and M.S. degrees in applied meteorology from the Nanjing Institute of Meteorology, Nanjing, China, in 1985 and 1990, respectively, and the Ph.D. degree in applied remote sensing from Zhejiang University, Hangzhou, China, in 2000.

From 1985 to 1997, he was a Research Scientist with the Meteorological Institute of Xinjiang, Ürümqi, China. Since 2001, he has been a Professor with the College of Environmental and Resource Sciences, Zhejiang University. He has authored eight books and more than 250 research articles. His research interests include remote sensing applications in natural resources and the environment.



Xiaodong Song received the B.S. degree in cartography from Wuhan University, Wuhan, China, in 1998, and the M.S. degree in cartography and geography information system from Wuhan University, in 2004, and the Ph.D. degree in cartography and geography information system from Nanjing University, Nanjing, China, in 2008.

He is an Associate Professor with the Zhejiang University of Water Resources and Electric Power, Hangzhou, China. His research interests include ecological modeling, climate change, and drought.



Huayang Wen was born in Shuyang County, Jiangsu, China, in 1983. He received the B.S. and M.S. degrees from the Hefei University of Technology, Hefei, China, in 2005 and 2008, respectively.

He is with the Anhui Meteorological Information Centre, Anhui Meteorological Bureau, Hefei, mainly engaged in meteorological data quality control and assessment, and product development.



Haiyu Song received the B.S. degree in mathematics and the Ph.D. degree in control theory and control engineering from the Zhejiang University of Technology, Hangzhou, China, in 2009 and 2015, respectively.

He is an Associate Professor with the School of Information Management of Artificial Intelligence, Zhejiang University of Finance and Economics, Hangzhou. His research interests include distributed estimation, security of cyber-physical systems, networked filtering, and information fusion.